Uncertainty and Sensitivity Analysis of Blunt Impact Tissue Response Using a Swine Finite Element Model

Final Technical Report No. J0511-18-726
Under Prime Contract N00174-17-C-0003

Prepared by
Jianxia Cui, PhD
Laurel Ng, PhD

L-3 Applied Technologies, Inc.
10180 Barnes Canyon Road
San Diego, California 92121

Prepared for
Terri Schull
2807 Strauss Avenue
Bldg. 695, Code R3C
Indian Head, MD 20640

December 12, 2018

Executive Summary

This report describes the uncertainty and sensitivity analysis of tissue response from non-lethal relevant impacts using a swine finite element model. A case study on projectile impact over the lung region was conducted. We used response surface methodology (RSM) and Latin hypercube sampling (LHS) for selecting the input parameters of the mechanical properties of muscle and skin, rib, and lung. The output responses were the peak energy density (PED), contact force, rib stress, and the lung contusion percentage for lung impact simulations.

In RSM, we used a face-centered central composite design (CCD) to select extreme cases for the FEM simulations and the quadratic regression fitting function in MATLAB to fit the response surface models to the output of FEM. We statistically analyzed the goodness of fit and the significance of the fitting coefficients with their p-values. We quantified the uncertainty with the cumulative distribution function (CDF), boxplot, histogram, mean and standard deviation for both methods. For sensitivity analysis, we used p-values and line plots drawn with the response surface models to identify which parameters had the greatest effect on tissue response, including higher order parameters and parameters that interacted with each other.

In LHS, 50 samples of input parameters were selected based on a truncated Gaussian distribution. We quantified the uncertainty with the CDF, boxplot, histogram, mean and standard deviation. We used scatter plots and rank correlation to analyze the sensitivity and calculated the coefficient of variation.

The LHS method provides more accurate uncertainty quantification than RSM, as it provides a better representation of the statistical spread of material properties. Uncertainty analysis showed that for lung impacts at 40 m/s, the contact force, rib stress, and contusion had relatively low normalized coefficient of variation values of ~0.08. The PED has a higher coefficient of variation of ~0.24. Thus, despite large variability in input tissue properties, the responses in general did not vary greatly, as reflected by the coefficient of variation. Uncertainty analysis at impact speeds of 20 m/s and 40 m/s resulted in similar coefficients of variation with the exception of the contusion, where the coefficient of variation increased as impact speed decreased.

The sensitivity analysis based on RSM and LHS confirmed one another for the lung impact under a projectile speed of 40 m/s. Specifically, the most sensitive parameters for PED, contact force, rib stress, and contusions were muscle-skin, rib, rib, and muscle-skin respectively. Based on RSM analysis, the contact force and contusion were most sensitive to the second order properties of muscle-skin. The PED, contact force, and contusion were most sensitive to the parameter interaction of muscle-skin and rib.

Futures studies will focus on uncertainty and sensitivity analysis of impact to the other regions and organs of the body.

Contents

Figures

Tables

1 Introduction

1.1 Background

Complex computational models (such as finite element models (FEMs)) typically contain a number of model parameters that are uncertain for various reasons; one such example are assigned mechanical properties of biological tissues, which inherently vary around an average value. Variability is inherent in bio-materials (such as tissues) that are used in biomechanical models. Despite parameter uncertainty, it is common practice to construct models that are deterministic in the sense that single numerical values, typically representative of the mean value, are assigned to each parameter. Hence, it is important to know how the uncertainty in the model parameters (inputs) affects the model predictions (outputs). To assess the variability in the simulated response given a range of realistic values, a sensitivity and uncertainty analysis is typically performed.

Uncertainty quantification is a means to quantify the uncertainty in the model responses (outputs of the model) that arise from uncertainty in the model parameters (input of the model). Instead of assuming fixed model input as in a deterministic model, one assigns a distribution of possible values to each model parameter. The uncertainty in the model parameters is then propagated through the model and give rise to a distribution in the model responses [1]. Sensitivity analysis is tightly linked to uncertainty quantification and is the process of quantifying how much of the output uncertainty each parameter is responsible for [2]. A small change in a highly (lowly) sensitive parameter of the model leads to a comparatively large (small) change in the model output. In this study, we use response surface methodology (RSM) and a sampling-based method called Latin hypercube sampling (LHS) method to conduct uncertainty and sensitivity analysis in a swine FEM.

RSM, a statistical method, explores the relationships between several explanatory variables and one or more response variables [3]. The main idea of RSM is to use a sequence of designed experiments or simulations using an approach called design of experiments (DOE) to obtain the relationships between the input and output and to find an optimal response. These designs are most effective when there are less than 5 factors (input parameters). The main advantage of using RSM is to understand and evaluate the effect of multiple parameters (inputs) and their interactions with each other in the responses (output).

Statistical DOE provides a quantitative and highly efficient approach to characterize and then optimize a multitude of input parameters (the optimization is not our focus in this study though). A DOE varies multiple factors simultaneously, and because each factor column in the experimental matrix is orthogonal with respect to the others, the factor's main effects, as well as the factor interaction effects can be estimated independently.

LHS [1, 4] is a statistical method for generating a near-random sample of parameter values from a multidimensional distribution. It is used to produce input values for estimation of expectations of functions of output variables. This technique requires fewer simulations to produce the same level of precision than the simple random sampling method and ensures that the upper and lower ends of the distributions used in the analysis are well represented [5]. Therefore, the total number of simulations required to preserve the probability distributions is greatly reduced [6] compared with the simple random sampling. The LHS is generally recommended over simple random sampling when the model is complex or when time and resource constraints are an issue [5].

1.2 Needs and Gaps

Literature [7] shows that the mechanical response of biological tissues can vary for a number of reasons including strain-rate dependence, age of the subject, and natural physiologic variability. Therefore, there is a need to investigate uncertainty in tissue responses due to natural variability in mechanical properties over a population. Also, it is important to understand which material properties have the greatest influence on the response that is being modeled, and identify relationships between the mechanical properties of the tissues (the inputs of interest) and the mechanical responses (the outputs of interest). Thus, sensitivity and uncertainty analysis is needed.

1.3 Objective

The objective of this study is to conduct sensitivity and uncertainty analyses using a swine FEM model. In this study, we explore the RSM and LHS methods to conduct the analysis. For RSM, we used a face-centered central composite design (CCD) to simulate the extremes cases in order to obtain the first primary sensitivity of different input parameters in the sense of contribution to the responses (i.e., which parameter(s) is (are) dominant parameters to different outputs), and to find if there is any interaction and/or higher-order effect. For LHS, we used a truncated Gaussian distribution round the mean mechanical tissue properties that are used in the original/base FE model. We also explored the parameter of projectile speed on model response.

2 Methods

2.1 Material Models Used in a Swine FEM

Using the Swine FEM model [8], we first analyzed tissue response to impact of the chest/lung region, which include the interaction of muscle-skin, ribs, and lung tissues. The material models used for these tissues in the swine FEM are listed in Table 1, the specific values that were used are described in 2.4 Latin Hypercube Sampling.

Table 1 Material models in Swine FEM

Material Component	Material Model	Model keyword in LS-DYNA
Muscle and Skin	Odgen rubber Material type 77	*MAT_OGDEN_RUBBER
Rib	Elastic Material type 1	*MAT_ELASTIC
Lung	Elastic Material type 10	*MAT_ELASTIC_PLASTIC_HYDRO

2.2 Response Surface Methodology (RSM)

RSM [9] is a collection of statistical and mathematical methods that are widely used to model and analyze complex problems. The main objective of RSM is to optimize the response surface that is influenced by various process parameters. RSM also quantifies the relationship between the controllable input parameters and the obtained response surfaces. RSM has been adopted in our study to express the output parameters (responses) that are influenced by the input parameters of material properties. RSM designs allow us to estimate interaction and quadratic effects, and therefore give us an idea of the (local) shape of the response surface under investigation.

RSM involves mathematical and statistical techniques that are used for modeling and analyzing the problem in which a response (output) is influenced by several input variables. The relationship between the input parameters and the response are expressed by multiple regression equations. If all variables are assumed to be measureable, the response surface can be expressed as a fitted model $y=f(x_1,x_2, \ldots, x_k)$. It is assumed that the independent variables are continuous and controllable by experiments with negligible errors. Usually a second-order model is utilized to find a suitable approximation for the functional relationship between independent variables and the response surface, showing as the following quadratic equation:

$$y = \beta_0 + \sum_{i=1}^{k} \beta_i x_i + \sum_{i}^{k} \beta_{ii} x_i^2 + \sum_{i} \sum_{j} \beta_{ij} x_i x_j \qquad (1)$$

Here, x_i and x_j represent different input parameters, y represents one of the responses that are interesting to us, and β represents the coefficient for each of the terms, specifically, β_i, β_{ii}, and β_{ij} are coefficients for first-order, second order and interaction effects. The solution of β can be obtained by the matrix approach. We used functions in the Statistics and Machine Learning Toolbox of MATLAB (The MathWorks, Inc.) to solve the equations (i.e., to get the best fit) and to evaluate the fitted results with statistical analysis.

The goodness of fit is measured by R-squared and adjusted R-squared. The former is the proportion of the variance in the dependent variable y that is predictable from the independent variable(s) (x). R-squared and adjusted R-squared can be calculated as follows:

$$R^2 = 1 - \frac{\sum_i (y_i - f_i)^2}{\sum_i (y_i - \bar{y})^2}; \quad \bar{y} = \frac{1}{n} \sum_{i=1}^{n} y_i$$

$$R_{adj}^2 = 1 - (1 - R^2) \frac{n-1}{n-p}$$

Here, n is the number of the observations, and p is the number of regression coefficients. (Note that p includes the intercept in MATLAB, otherwise, the denominator in adjusted R squared would be $n-p-1$, as defined in some other statistics tools). The adjusted R-squared can be negative, its value will always be less than or equal to that of R-squared. The larger R-squared is, the more variability is explained by the regression model (i.e., the larger R-squared is, the better the predication model is). Because R-squared increases with added predictor variables in the regression model, the adjusted R-squared adjusts for the number of predictor variables in the model. This makes it more useful for comparing models with a different number of predictors.

The design procedure of RSM is: 1) design a series of experiments (i.e., simulations) for adequate measurement of the response of interest (output) (see Section 2.3); 2) develop the mathematical model of the second order response surface with the best fit to find the relationships between the output (tissue responses) and input parameters; 3) evaluate the fitted results with statistical tests; and 4) visualize the direct and interactive effects of input parameters on the output (see Results).

2.3 Design of Experiment for RSM

RSM involves some unique experimental design considerations due to the emphasis on iterative experimentation and the need for a relatively sparse design that can be built-up piece-by-piece according to the evolving needs. Among the designs, Box-Behnken and central composite designs

(CCD) are efficient and standard designs for fitting second order polynomials to response surfaces because they use a relatively small number of observations to estimate the parameters [10]. The general purpose of the RSM is to optimize a process or system (although it is not the purpose for this study). However, the location of optimum is usually unknown prior to running the experiment (simulation), so it makes sense to use a design that provides equal precision of estimation in all directions. For such purposes, spherical or face centered CCD and Box–Behnken design are commonly used experimental design models for three-factor experiments.

In our study of uncertainty and sensitivity analysis in a swine FEM, we used a face centered CCD to simulate 19 extreme cases with three different values (-1, 0, and 1) for three input parameters that represent the properties of muscle and skin, rib, and lung (e.g., softest = -1, base = 0, and stiffest = 1). Table 2 shows the parameters used in the 19 simulations designed with a face-centered CCD. Each column represents the array (vector) that stands for the specific material properties.

Figure 1 illustrates the cube representation of a three-factor CCD face-centered DOE matrix. The center of the CCD represented by Case #1 (Table 2), in which all material properties were set to 0 (i.e., the base condition), is represented by the center gray ball in Figure 1. The arrays in CCD are orthogonal to each other. Two vectors are orthogonal if the sum of the products of their corresponding elements is 0.The gray balls on the 6 surfaces represents axial points, and their distance to the center gray ball (base condition) is set to 1 in face centered CCD. The red balls are factorial points. We added 4 more cases that are not in CCD, still meeting the orthogonal requirement in order to have more data points to do further uncertainty and sensitivity analysis.

Table 2 Input Parameters for 19 Extreme Cases

Case #	Muscle-Skin	Rib	Lung
1	0	0	0
2	0	0	-1
3	0	0	1
4	-1	0	0
5	1	0	0
6	0	1	0
7	0	-1	0
8	1	1	0
9	1	1	-1
10	1	1	1
11	-1	-1	0
12	-1	-1	-1
13	-1	-1	1
14	1	-1	0
15	-1	1	0
16	1	-1	-1
17	1	-1	1
18	-1	1	-1
19	-1	1	1

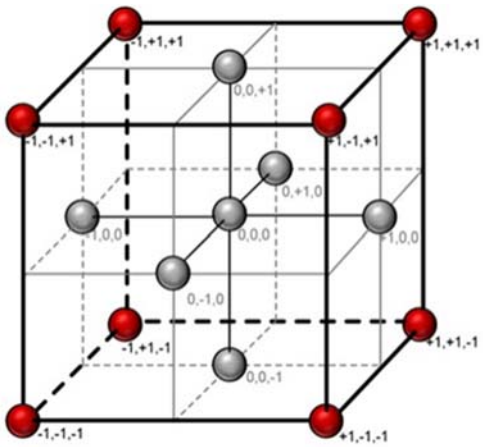

Figure 1 Cube representation of a three-factor CCD face-centered DOE matrix (adopted from [11]). The numbers of -1, 0, and 1 represent softest, base, and stiffest materials, respectively, for the three factors of muscle-skin, rib, and lung. The gray balls on the 6 surfaces represent axial points, their distance to the center gray ball (base condition) is set to 1 in face centered CCD. The red balls are factorial points.

2.4 Latin Hypercube Sampling

To obtain a Latin hypercube sample, the input variables are assumed to be truncated Gaussian distributions over the range of [-1 1] for each of the input parameters. The range is divided into n intervals of equal probability ($1/n$), and one value is randomly picked from each interval [1, 4]. Then n values for the k input variables are formed strategically (see next paragraph) into a n by k matrix. The number n of simulations (sample size) depends on the number k of input variables (k = 3 in our case). It is suggested that the number of simulations be between 4/3 to 5 times the number of input variables [6]. Additionally, the acceptable sample size n also depends on the quantiles. For estimating the 0.95 quantile from the cumulative distribution function (CDF), a sample size of at least 20 is required [6]. For our study, a sample size of 50 (n = 50) is considered in the uncertainty and sensitivity analysis. Figure 2 shows the CDF and the probability density function (PDF) taking rib variables as the example. The equations that define this distribution is given as the follows:

$$\mu = 0;$$
$$\sigma^2 = 0.2;$$
$$quantile = \mu + \sigma\sqrt{2}erf^{-1}(2F - 1);$$
$$F = \frac{1}{2}\left[1 + erf\left(\frac{x - \mu}{\sigma\sqrt{2}}\right)\right];$$
$$pdf = \frac{1}{\sqrt{2\pi\sigma^2}}e^{-\frac{(x-\mu)^2}{2\sigma^2}};$$

The distribution is a truncated Gaussian distribution $N(0, \sqrt{0.2})$. The CDF and PDF figures are plotted against a standard normal (Gaussian) distribution in Figure 2. The values shown

in black squares are used in FEM simulations. Note that the formulation above results in edge points that extend slightly below -1 or above -1. To maintain consistency with the desired range of -1 to 1 for analysis, values that fall below -1 are taken as -1 and values that fall above 1 are taken as 1. Similar treatment of data was used for muscle and skin and lung properties. Figure 3 shows correlations for pairs of the three input parameters.

It is not trivial to form a n by k matrix that can act well in the estimation and prediction of uncertainties and sensitivities, and different algorithms (called Latin hypercube design, LHD) for designing such a good matrix have been proposed and used in different fields [12]. Usually a good LHD would make the correlation between the input variables close to the minimum and the sample space uniformly filled. To form an optimal LHD for 50 LH samples of 3 input parameters (a 50 by 3 matrix), we followed these steps:

1. Randomly generate multiple Latin hypercube samples by using various seed values in MATLAB.
2. Find the maximum absolute rank correlation coefficient (RCC) value amongst all two-variable pairs from each sample. The RCC measures the strength of the monotonic relationship between two variables [1]. In this case, with 3 input variables, there are 6 such pairs and hence 3 RCC values from each sample.
3. Adopt the sample with the minimum absolute RCC value amongst those maximum absolute RCC values.

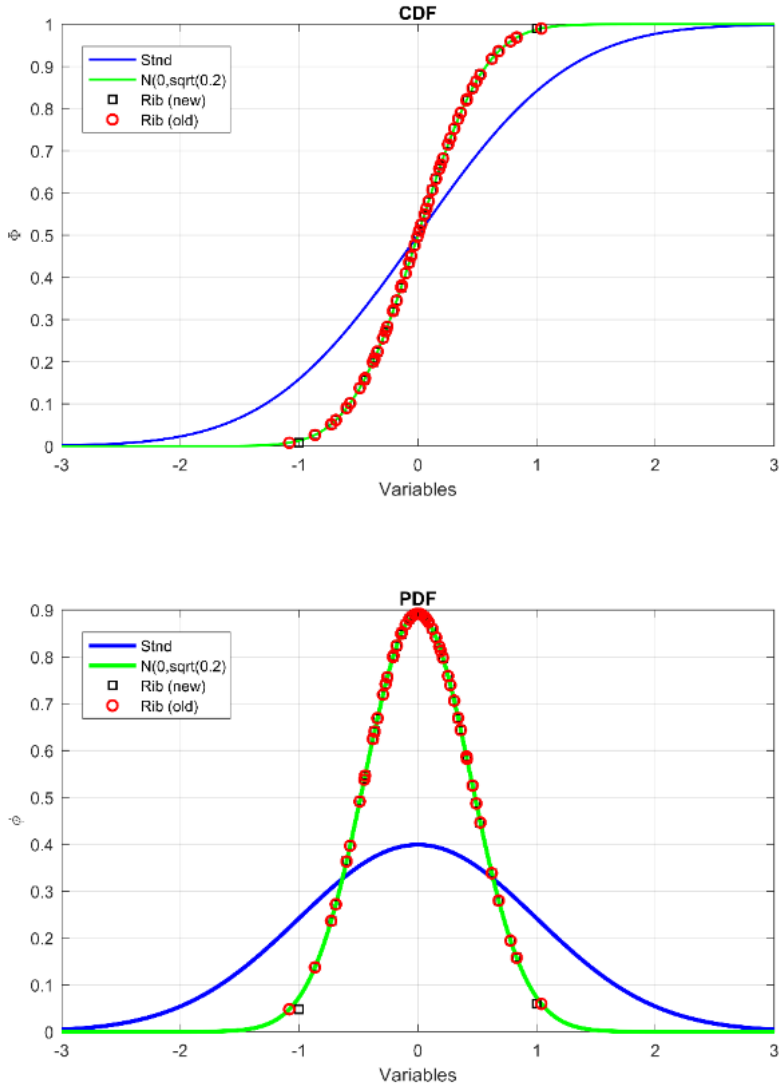

Figure 2 The CDF (top) and PDF (bottom) of truncated Gaussian of N(0,sqrt(0.2)) (green lines) for Rib variable (red circles and black circles) comparing with a standard normal (Gaussian) distribution (blue line). Note that black squares are the same as the red circles except that the values that fall below -1 or fall above 1 for red circles are taken as -1 and 1 for black squares. The values shown in black squares are used in FEM calculations. Similar data treatment was used for muscle-skin and lung properties.

The relationship between three pairs of 3 variables are shown in Figure 3. The RCC values and its *p*-values are denoted by R and P respectively in the title of the subplots. Note that R=1 indicates a positive linear correlation whereas R=-1 a negative linear correlation between the variables. R=0 indicates that there is no correlation between the two variables. A less than 0.05 *p*-value means a significant correlation between the two variables. The values of R and P shown in Figure 3 indicate the paired variables are not correlated, which is the goal in developing an optimal LHD for uncertainty and sensitivity analysis. The values represented by the black squares are used in the FEM simulations As shown in Figure 3, these values have an lower correlations (lower R and higher P) than the one represented by red circles.

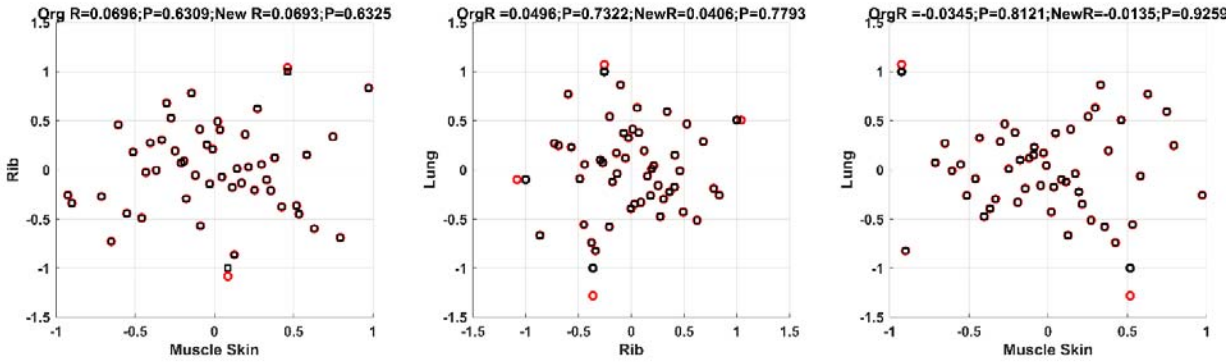

Figure 3 The correlation between paired input variables, here MS denotes muscle and skin. The RCC and its *p*-values are shown by R and P in the title. Note that black squares are the same as the red circles except that the values that are a little less than -1 or a little greater than 1 for red circles are taken as -1 and 1 for black squares. The values shown in black squares are used in FEM calculations. The R and P values after "Org" are for red circles, and after New are for black squares.

With these values for the three parameters obtained with LSD, we calculated the parameters that control the properties of muscle-skin, rib, and lung based on the equations given in Table 3. The parameters of Mu1, G1, G2, E, and C1 are the specific parameters for each material type defined in the LS-DYNA Keyword User's Manual (Livermore Software Technology Corporation, LSTC). Note that *x* is the model index from the model in the first column of Table 3, as defined in Table 2 (and also Figure 3) that -1, 0, and 1 represent the softest, base, and stiffest properties, respectively, which were based on the published literature values [7]. The equations in the second column of Table 3 were fit using the literature values. Figure 4 shows an example of stress – strain for muscle-skin properties. The black solid curve indicates the base value for muscle-skin; the softest and stiffest curves correspond to the dash-dotted line and dashed line, respectively. The remaining lines are data from literature.

Table 3 Model Equations for material models used in FEM

Model	Equations and constants
Muscle-Skin	Mu1=G1=a*exp(b*x) G2=p2*x^2+p1*x+p0 a=29.59; b=2.093, p2=1.25, p1=4.75, p0=4
Rib	E = 10+4*x
Lung	EOS equation: C1= a*exp(b*x), a=103.5, b=1.574

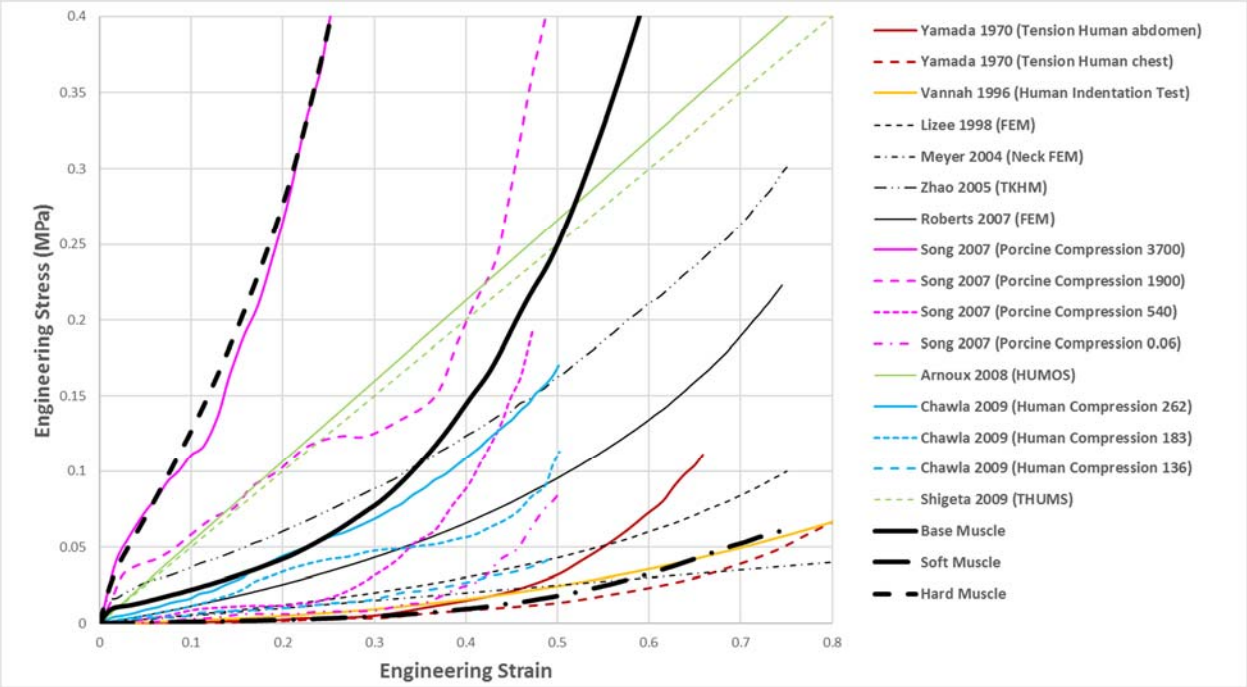

Figure 4 Muscle stress-strain properties. The black solid curve indicates the base value for muscle-skin. The softest and hardest curves correspond to the dash-dottted line and the dashed line, respectively. The remaining curves are data from literature.

3 Results

3.1 Results from Response Surface Methodology

The projectile speed was set to 40 m/s in the FEM simulations for the RSM analysis. The material properties were set either as softest, stiffest or base as indicated in Methods.

3.1.1 Response results from the extremely cases selected by CCD

The peak energy density (PED), contact force, rib stress, and contusion percentage are the output parameters (responses) in which we are interested for the simulations of the 19 extreme cases. The results for each run are given in Table 4 , and Figure 5-Figure 8. Figure 5 shows the uncertainty of PED through the CDF (top panel), boxplot (middle panel), and histogram (bottom panel). The black dots in the CDF and boxplot represents the mean value of PED. The median value (50^{th} percentile) of the PEDs from the 19 simulations is shown by the red bar in the boxplot. The edges of the boxplot represent the 25th and 75th percentiles (i.e., the 1st and the third quantiles, Q1 and Q3). The difference between the first and third quantiles is called the interquantile range (IQR). The maximum (the upper extreme) of the boxplot is calculated as: Q3+1.5IQR, the minimum (lower extreme): Q1-1.5IQR. The whiskers are the values between the box edges and the upper and the lower extremes. All the values larger/smaller than the upper/lower extreme are considered outliers. The base value, when all the 3 input parameters were set to 0, is shown by the red dot in the boxplot.

The histogram shows the occurrence frequency of the PED. Similarly, Figure 6, Figure 7, and Figure 8 show the uncertainty analysis for percentage of lung contusion, contact force, and rib stress, respectively.

Table 4 Response Results for 19 Extreme Cases

Case#	Peak Energy Density (kPa)	Contact Force (kN)	Rib Stress (MPa)	Contusion Percentage
1	347.70	4.16	211.90	49.75
2	395.55	4.18	213.51	51.87
3	347.25	4.22	212.45	46.82
4	655.33	5.10	216.03	63.15
5	196.33	5.23	226.85	45.65
6	368.19	4.52	241.77	46.27
7	473.79	3.74	174.92	54.86
8	177.74	5.57	258.46	41.15
9	271.14	3.96	193.55	43.23
10	193.75	5.66	262.87	44.22
11	702.00	4.49	175.12	65.03
12	710.60	4.47	175.53	65.55
13	578.28	4.50	175.90	66.40
14	250.07	4.84	183.88	52.12
15	554.80	5.46	241.25	60.69
16	272.75	4.83	183.87	51.43
17	215.08	4.89	182.99	54.58
18	609.11	5.45	242.48	61.32
19	422.00	5.51	242.13	63.61

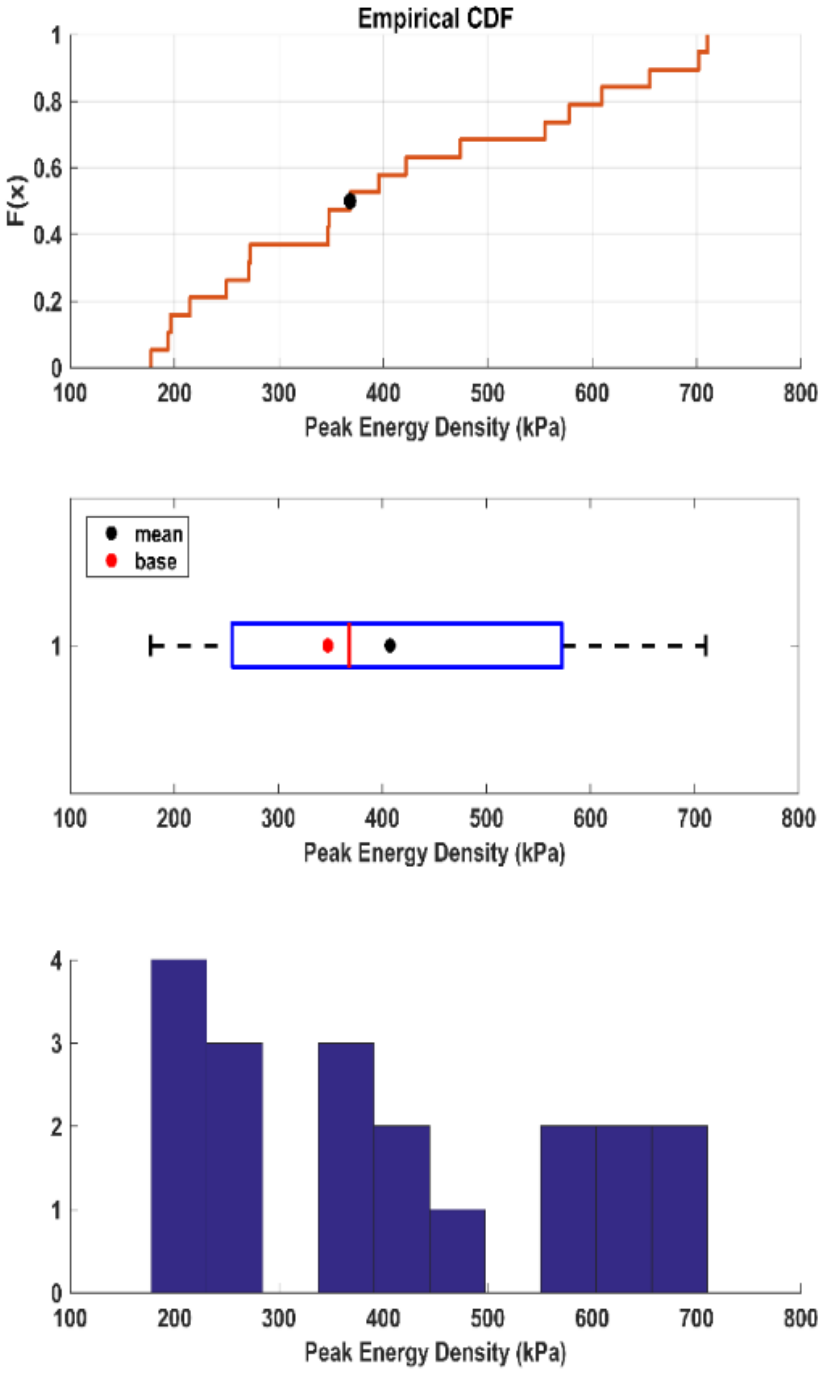

Figure 5 The uncertainty analysis for peak energy density (PED) with RSM. The black dots in the CDF and boxplot represents the mean value of PED. The median value of the PEDs from the 19 simulations is shown by the red bar in the boxplot. The base value, when all the 3 input parameters were set to 0, is shown by the red dot in the boxplot. The histogram shows the occurrence frequency of the PED.

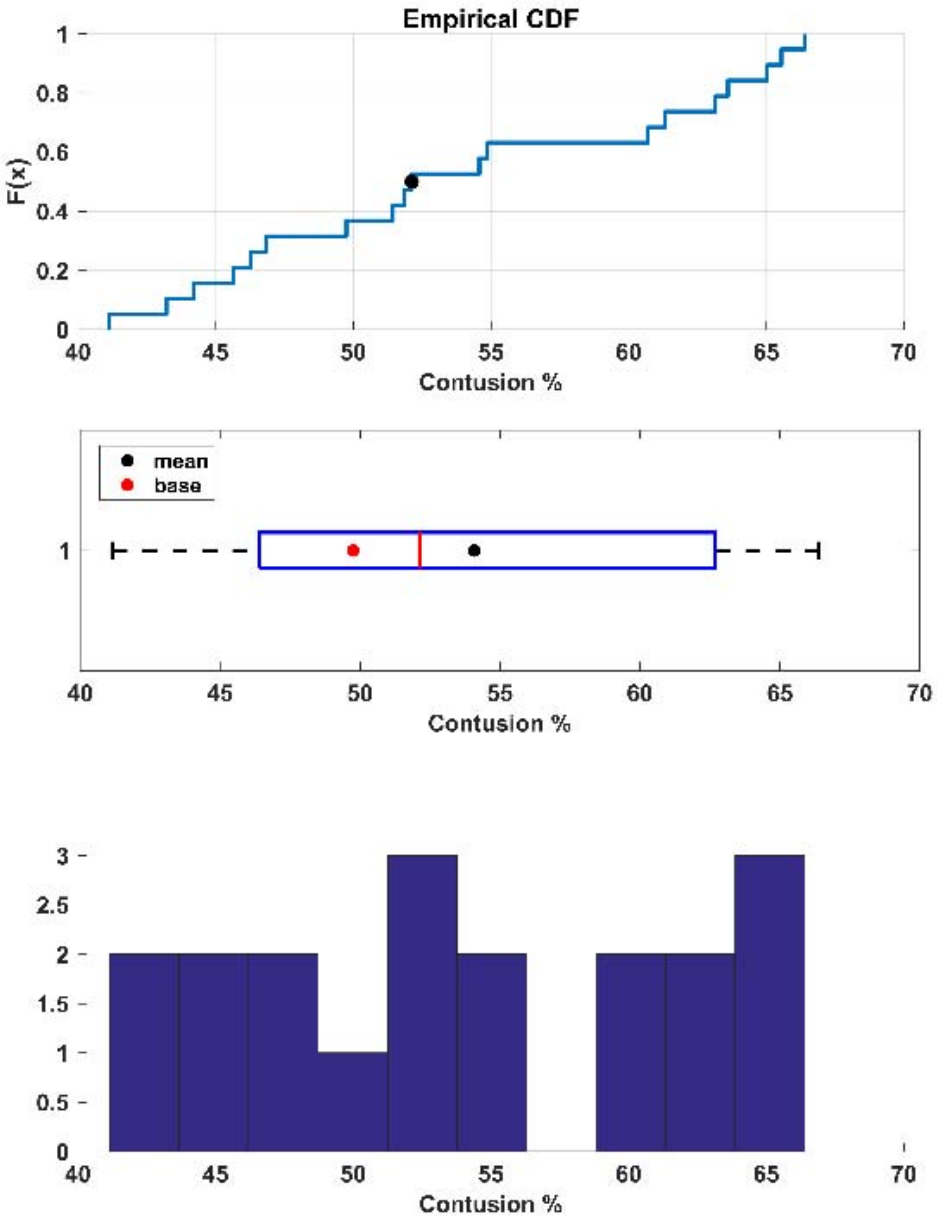

Figure 6 The uncertainty analysis for the percentage of lung contusion with RSM. The black dots in the CDF and boxplot represents the mean value of PED. The median value of the PEDs from the 19 simulations is shown by the red bar in the boxplot. The base value, when all the 3 input parameters were set to 0, is shown by the red dot in the boxplot. The histogram shows the occurrence frequency of the PED.

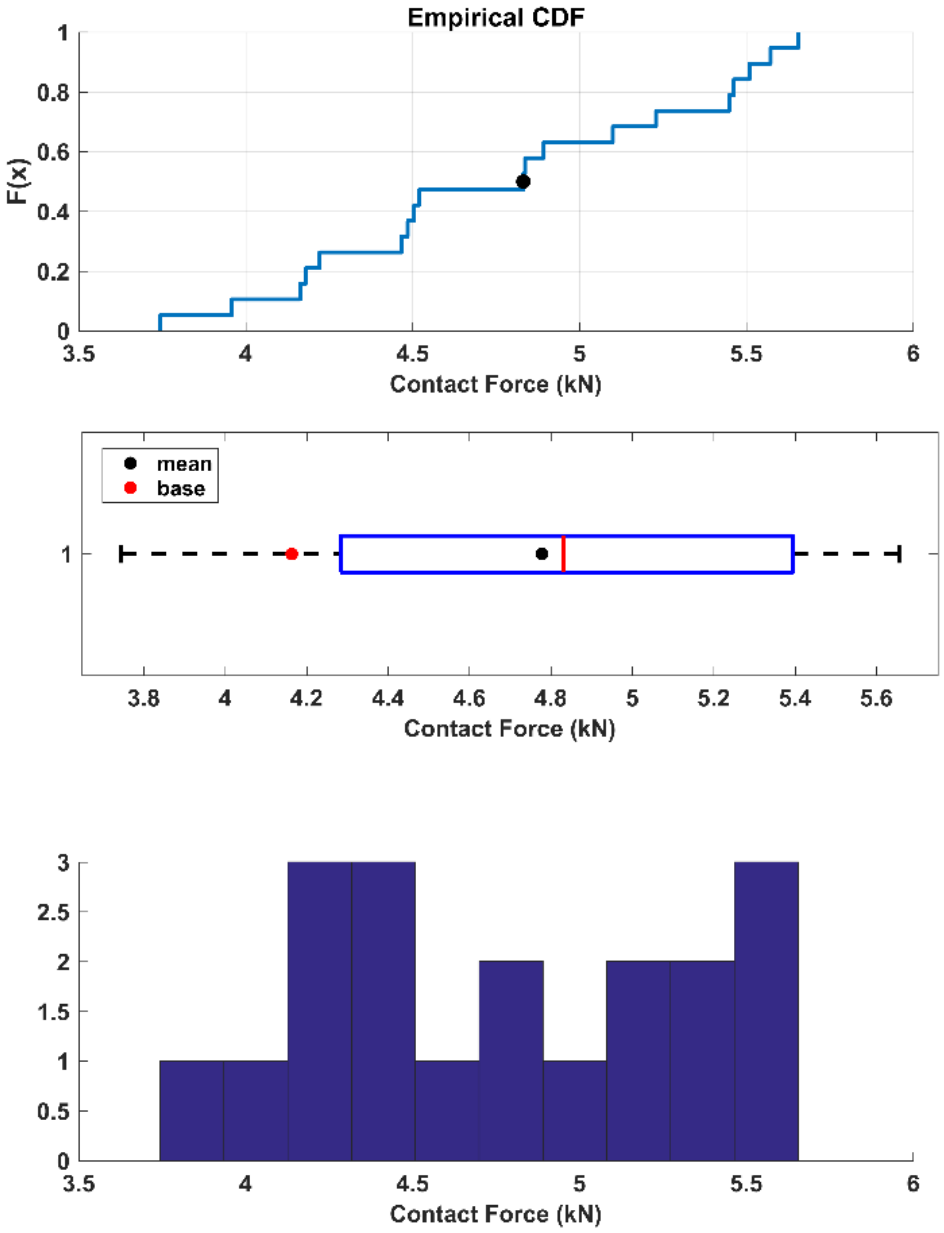

Figure 7 The uncertainty analysis for contact force with RSM. The black dots in the CDF and boxplot represents the mean value of PED. The median value of the PEDs from the 19 simulations is shown by the red bar in the boxplot. The base value, when all the 3 input parameters were set to 0, is shown by the red dot in the boxplot. The histogram shows the occurrence frequency of the PED.

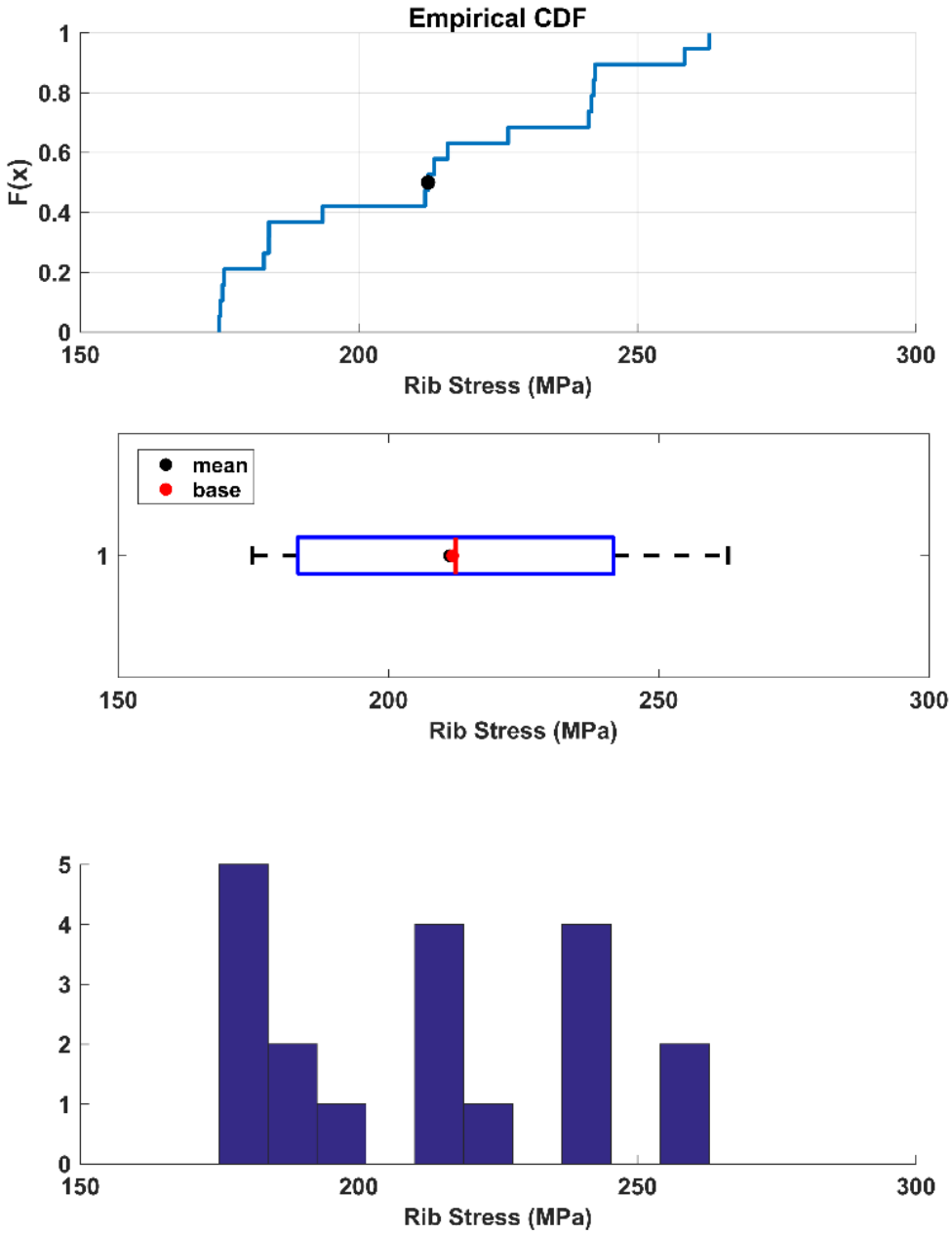

Figure 8 The uncertainty analysis for Rib Stress with RSM. The black dots in the CDF and boxplot represents the mean value of PED. The median value of the PEDs from the 19 simulations is shown by the red bar in the boxplot. The base value, when all the 3 input parameters were set to 0, is shown by the red dot in the boxplot. The histogram shows the occurrence frequency of the PED.

3.1.2 Sensitivity Analysis with the Response Surface Methodology

RSM involves mathematical and statistical techniques that are used for modeling and analyzing the problem in which a response (output) is influenced by several input variables. Given the input (Table 2) and the responses in which we are interested (Table 4), the relationship between the input

parameters and each of the responses could be expressed as equation (1), which was solved by functions in Statistics and Machine Learning Toolbox in MATLAB (MathWorks, Inc). In other words, the coefficients in equation (1) were predicted using MATLAB functions, and a response surface was fitted at the same time.

The goodness of fit is measured by ordinary R-squared and adjusted R-squared (Table 5). These values indicate that the fitted models are good. The larger the R-squared, the greater variability is explained by the regression model.

Table 5:Goodness of Fit for RSM

	Peak Energy Density (kPa)	Contact Force (kN)	Rib Stress (MPa)	Contusion Percentage
Ordinary R-squared	0.98	0.88	0.92	0.98
Adjusted R-squared	0.95	0.76	0.84	0.96

The *p*-value of the fitted coefficients indicates how strongly the input parameter(s) affect the responses; particularly a small *p*-value (<0.05) infers that there is a significant association between the parameter and the response. The *p*-values of the coefficients are given in Table 6, the *p*-values that are smaller than 0.05 are in bold, indicating the corresponding parameter(s) and interactions are significant, and they are important parameters to the response listed in the top row. The notations of *MS: Rib, MS:Lung,* and *Rib:Lung* in the first column indicate the interaction between the three parameters of MS, Rib, and Lung (e.g., *MS:Rib* indicates interaction effect between MS and Rib). The second order effect is indicated by *MS^2, rib^2, and Lung^2*.

Table 6 P-values of the Fitted Coefficients for the Parameters and Responses

Parameter	Energy Density (kPa)	Contact Force (kN)	Rib Stress (MPa)	Contusion Percentage
MS	**1.90E-08**	9.99E-01	6.08E-01	**2.91E-08**
Rib	**2.32E-03**	**2.94E-03**	**5.45E-06**	**3.16E-05**
Lung	**2.60E-03**	6.76E-02	1.12E-01	6.93E-01
MS:Rib	**4.57E-02**	**4.42E-02**	4.23E-01	**1.41E-02**
MS:Lung	1.25E-01	7.28E-02	7.66E-02	8.42E-01
Rib:Lung	5.12E-01	7.30E-02	7.29E-02	8.87E-01
MS^2	3.35E-01	**4.64E-04**	4.86E-01	**8.46E-04**
Rib^2	4.41E-01	4.87E-01	2.94E-01	2.88E-01
Lung^2	3.45E-01	3.66E-01	3.50E-01	2.95E-01

Plotted in Figure 9, Figure 10, Figure 11, and Figure 12 are the tissue responses (PED, contact force, rib stress, and contusion percentage, respectively) in relation to the properties of muscle-skin, rib, and lung given in the 19 cases (Table 4). The trend of variation shows agreement with the *p*-value analysis, the latter of which provides insight into contributions of the input parameters to the output (i.e., the sensitivity).

As indicated by the *p*-values in Table 6, the PED response showed greatest dependence on the properties of muscle-skin, followed by the properties of rib and of lung. In addition, the interaction *(MS:Rib*) between muscle-skin (MS) and the rib has a corresponding *p*-value less than 0.05, indicating a strong connection of PED to this interaction. Overall, the PED decreases significantly when the muscle-skin properties increase in stiffness, and, almost negligibly, as the properties of rib and lung vary, as indicated by Figure 9**.**

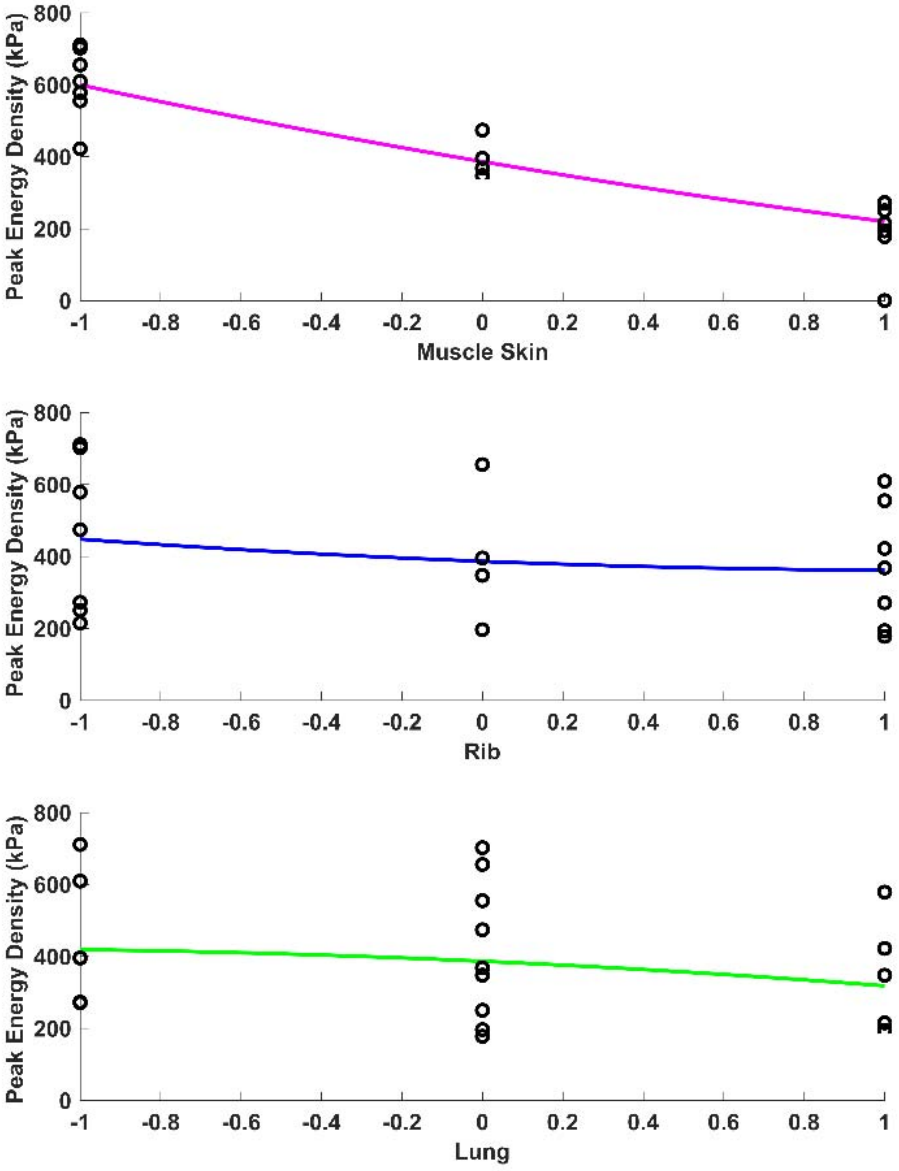

Figure 9 Fitted trend lines from RSM analysis for output of PED. The effect of muscle and skin, rib, and lung on PED is shown in the panels from the top to the bottom. The circles represent the 19 cases that were calculated in the FEM simulation.

Based on the *p*-values (Table 6), the most sensitive parameter to the peak contact force is the second order of the muscle-skin parameter. The rib material parameter is the second most influential parameter on the contact force. The contact force is also sensitive to the interaction of muscle-skin and rib (*MS:Rib*). Figure 10 illustrates that the peak contact force increases when muscle-skin properties move away from the base to the stiffest or to the softest extremes (second order effect). This behavior likely reflects the dominance of the stiff rib properties at the very soft MS range, and vice versa when the MS is very stiff. Peak contact force increases when the properties of rib vary from soft to stiff. Lung properties have little effect on the peak contact force.

The only sensitive parameter in the rib stress response is the property of rib, as indicated with the *p*-values in Table 6. Figure 11 illustrates that rib properties play a significant role in determining peak rib stress. The other two parameters (muscle-skin and lung) have no effect on the rib stress.

Contusion percentage is calculated by the volume of tissue that exceeds a defined peak energy density threshold (0.035 for moderate injury). The most sensitive parameter for contusion is the muscle-skin property, followed by the rib property, the second order of muscle-skin (*MS^2*), and the interaction of rib and muscle (*MS:rib*), as indicated by the *p*-values (Table 6). Figure 12 shows that contusion percentage decreases dramatically as muscle-skin properties vary from soft to stiff, and decreases as rib properties increase from soft to stiff. Variation of lung properties does not affect lung contusion percentage.

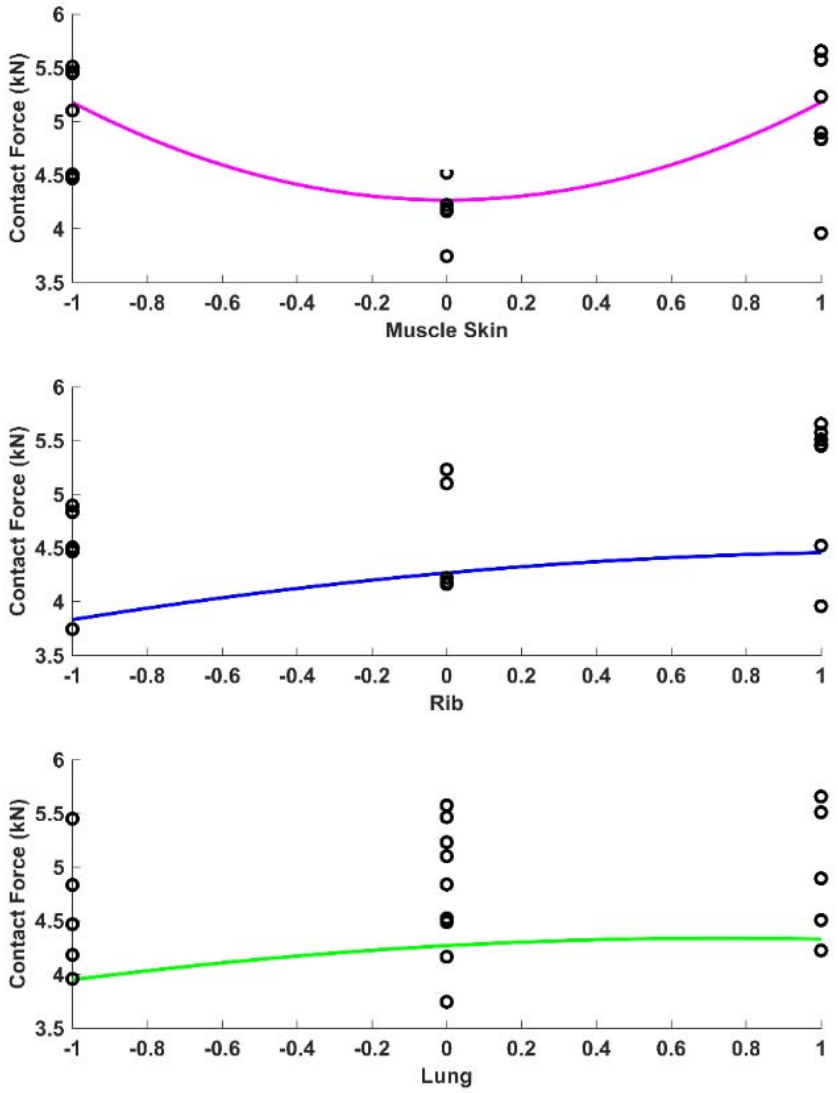

Figure 10 Fitted trend lines from RSM analysis for output of peak contact force. The effect of muscle and skin, rib, and lung on peak contact force is shown in the panels from the top to the bottom. The circles represent output from the 19 CCD cases that were calculated in the FEM simulation.

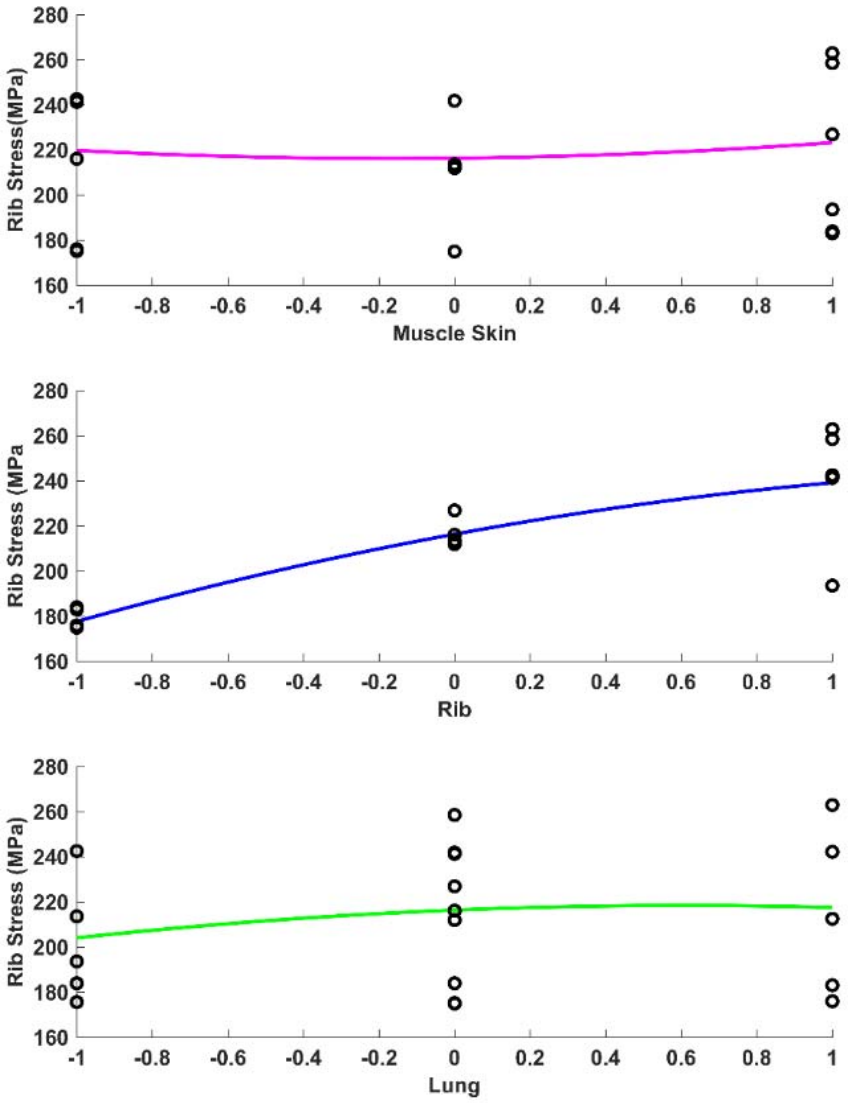

Figure 11 Fitted trend lines from RSM analysis for output of peak rib stress. The effect of muscle and skin, rib, and lung on peak rib stress is shown in the panels from the top to the bottom. The circles represent output from the 19 cases that were calculated in the FEM simulation.

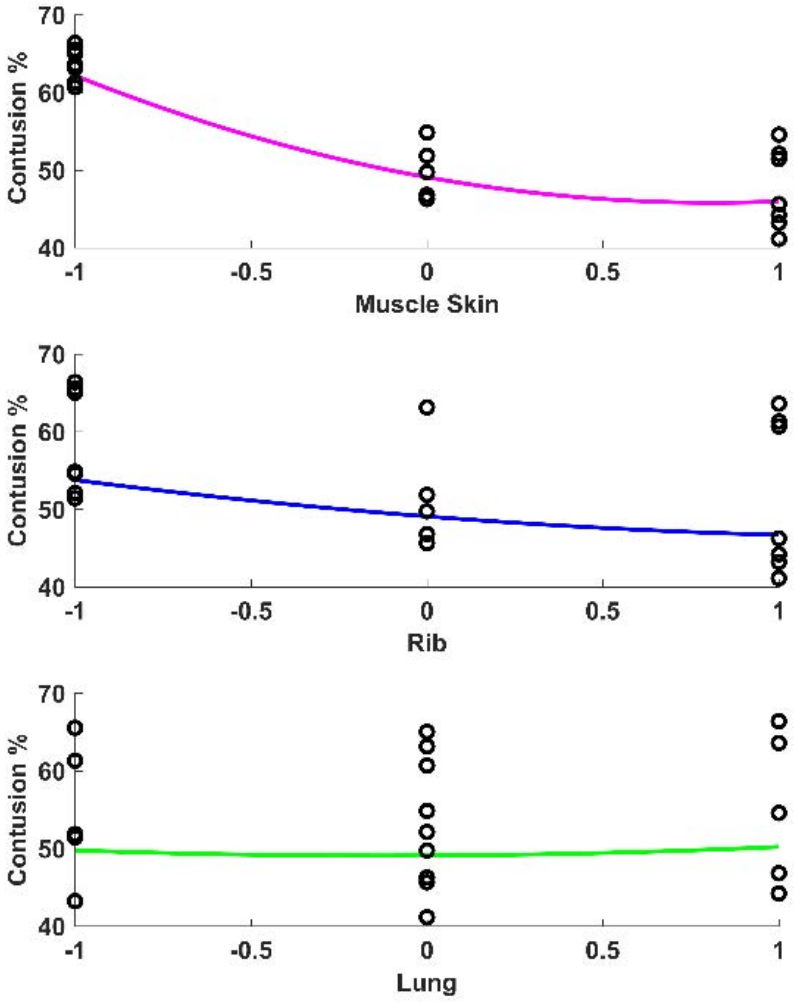

Figure 12 Fitted trend lines from RSM analysis for output of contusion percentage. The effect of muscle and skin, rib, and lung on contusion percentage is shown in the panels from the top to the bottom. The circles represent output from the 19 cases that were calculated in the FEM simulation.

3.2 Uncertainty and Sensitivity Analysis with Latin Hypercube Sampling

For uncertainty analysis, the uncertainty in model outputs due to the variability in model inputs is investigated with CDFs, boxplots, and histograms [13]. For sensitivity analysis, scatter plots and a ranking of the model's input with respect to their contribution to model output variability is provided.

3.2.1 Latin Hypercube Sample

Truncated Gaussian distributions for muscle-skin (denoted as MS), rib, and lung representing the stiffness (varying from the softest (-1) to the stiffest (1)) used for this analysis are shown in the

first 3 panels of Figure 13. Note that each value that falls within the range of -1 to 1 corresponds to one stress-strain curve (see Figure 4 for an example of muscle-skin) that lies between the softest and the stiffest curves for the specific tissue. The variation adjusts the moduli that characterize the material (e.g., shear moduli (G1, G2, Mu), Young's Modulus (or elastic modulus) (E), and Compliance (C)). See Table 3 for calculations of these moduli. The distribution of the moduli are plotted in the remaining panels of Figure 13. The distributions of these parameters vary depending on the equations used to calculate them.

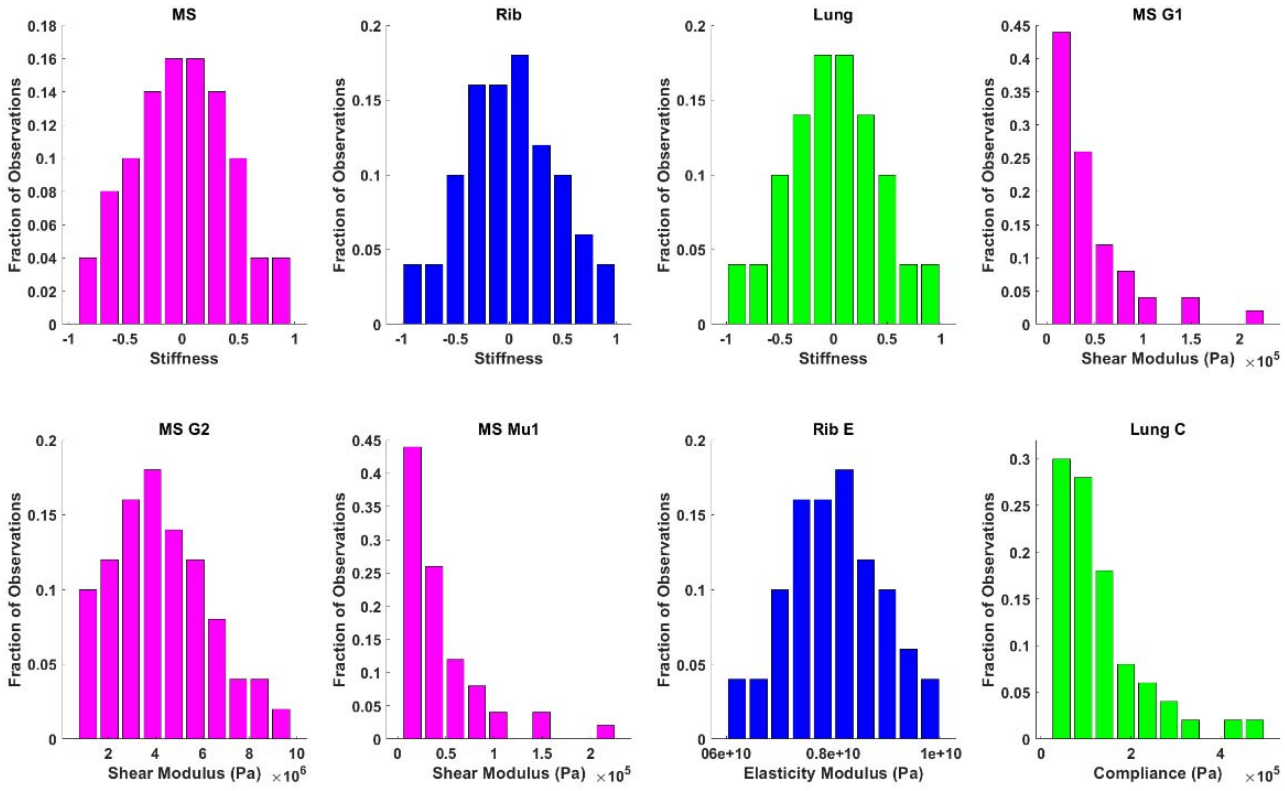

Figure 13 The uncertainty in the model material properties, indicated in the titles of the subplots (see Table 3), characterized in a histogram (in terms of fraction of observations). The material properties of MS, Rib, and Lung are color coded to the moduli that are related to each of the materials.

3.2.2 Uncertainty of the Responses

The FEM was simulated for the 50 truncated Gaussian distributed material models (Section 3.2.1) for a 40 m/s projectile impact. The CDFs, boxplots, and histograms for PED, contact force, rib stress, and contusion percentage are given in Figure 14, Figure 15, Figure 16, and Figure 17. The values for mean and standard deviation are given in the title of the subfigure with the histograms. The mean is also indicated with the black dots in the CDFs and boxplots. Because of the nonlinear relationship among the parameters used in FEM (Table 3 and Figure 13), the histograms of PED (Figure 14), contact force (Figure 15), and contusion percentage (Figure 17) do not follow a normal (Gaussian) distribution.

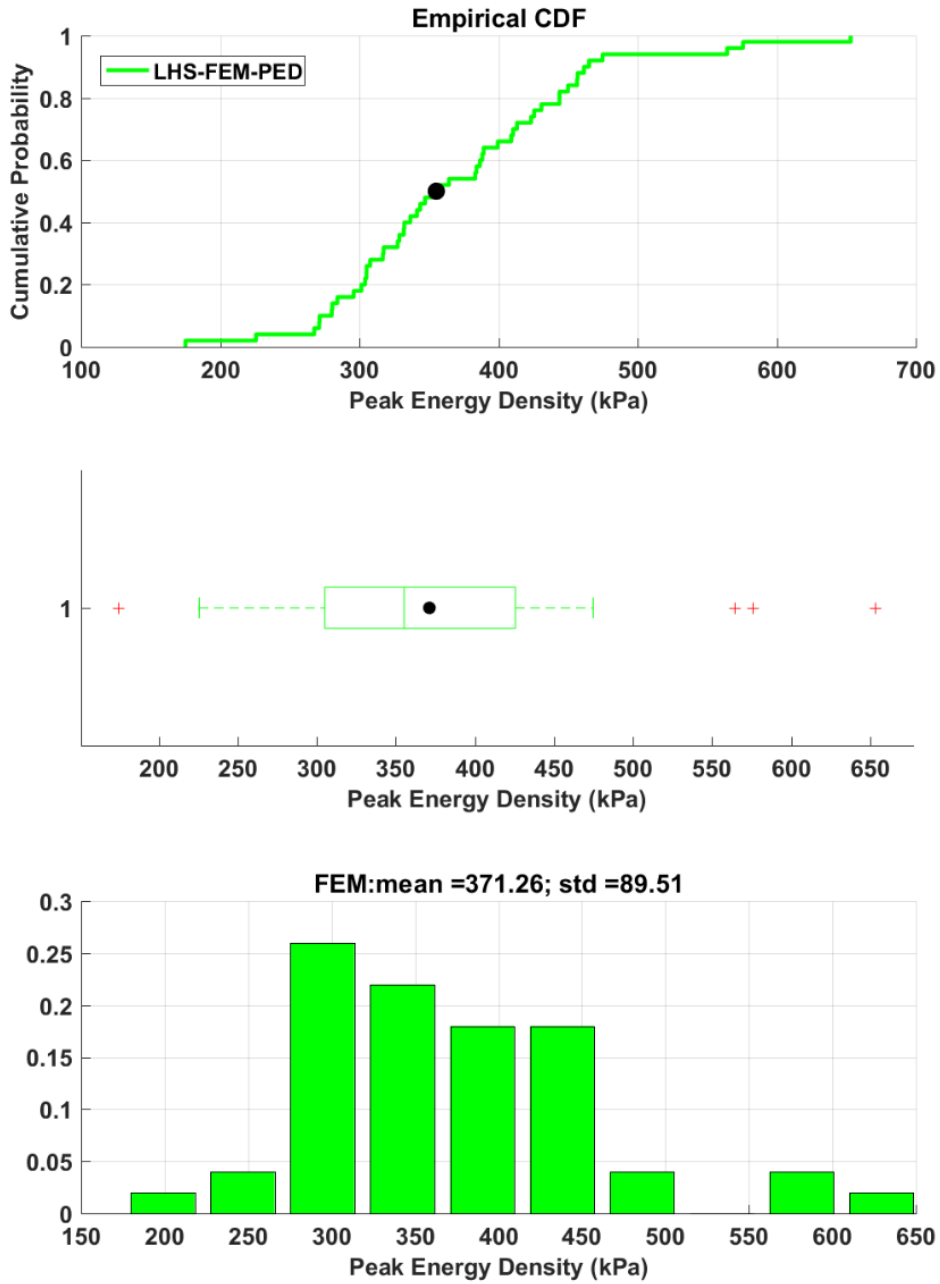

Figure 14 The uncertainty analysis with CDF, boxplot, and histogram for peak energy density (PED) based on the 50 FEM simulations. The values for mean and standard deviation are given in the title of the subfigure with the histogram. The mean is also indicated with the black dots in the CDFs and boxplots.

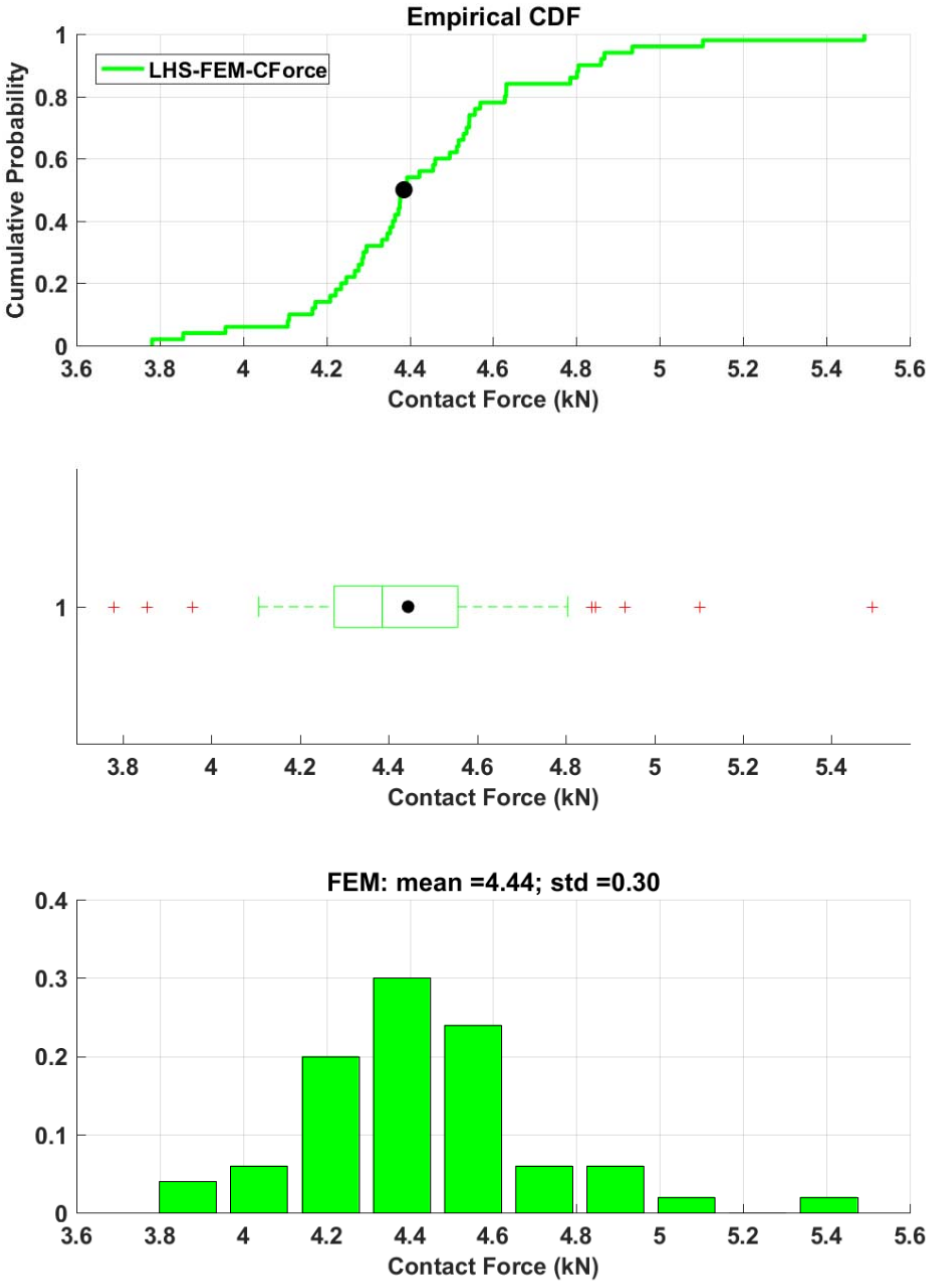

Figure 15 The uncertainty analysis with CDF, boxplot, and histogram for contact force based on the 50 FEM simulations subject to the LHS inputs. The values for mean and standard deviation are given in the title of the subfigure with the histogram. The mean is also indicated with the black dots in the CDFs and boxplots.

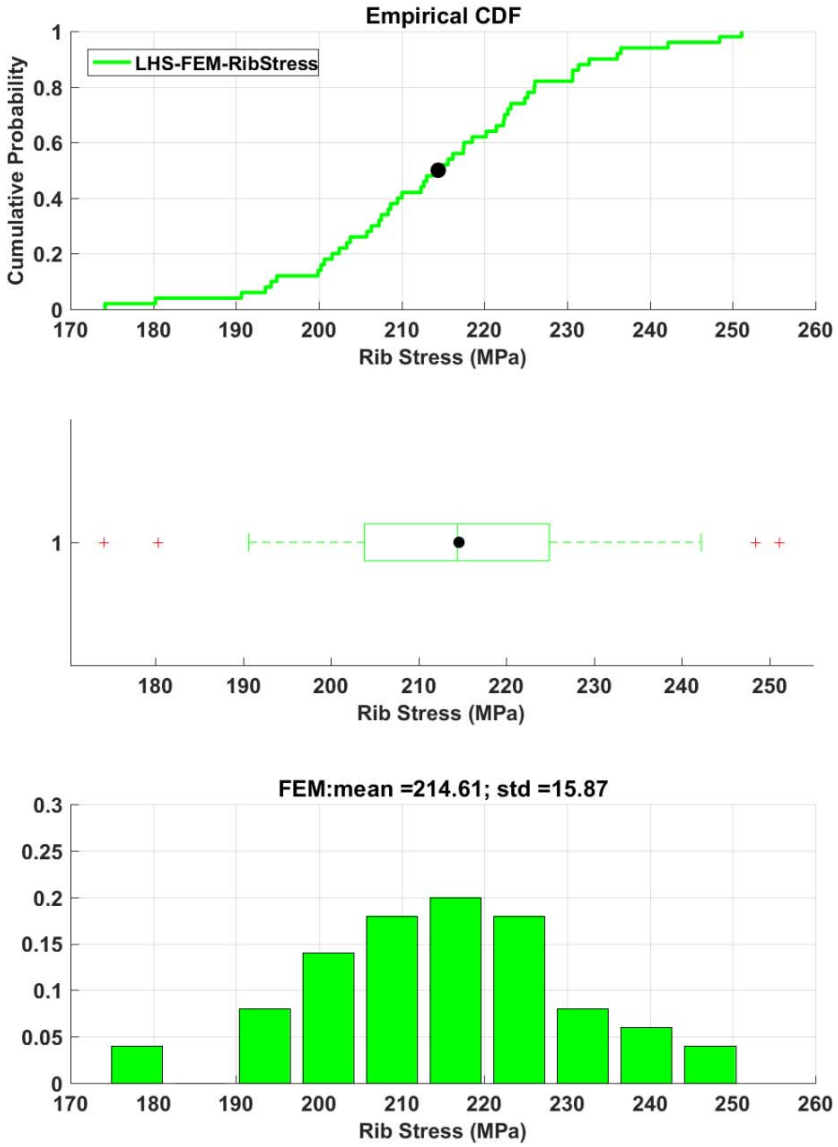

Figure 16 The uncertainty analysis with CDF, boxplot, and histogram for rib stress based on the 50 FEM simulations subject to LHS inputs. The values for mean and standard deviation are given in the title of the subfigure with the histogram. The mean is also indicated with the black dots in the CDFs and boxplots.

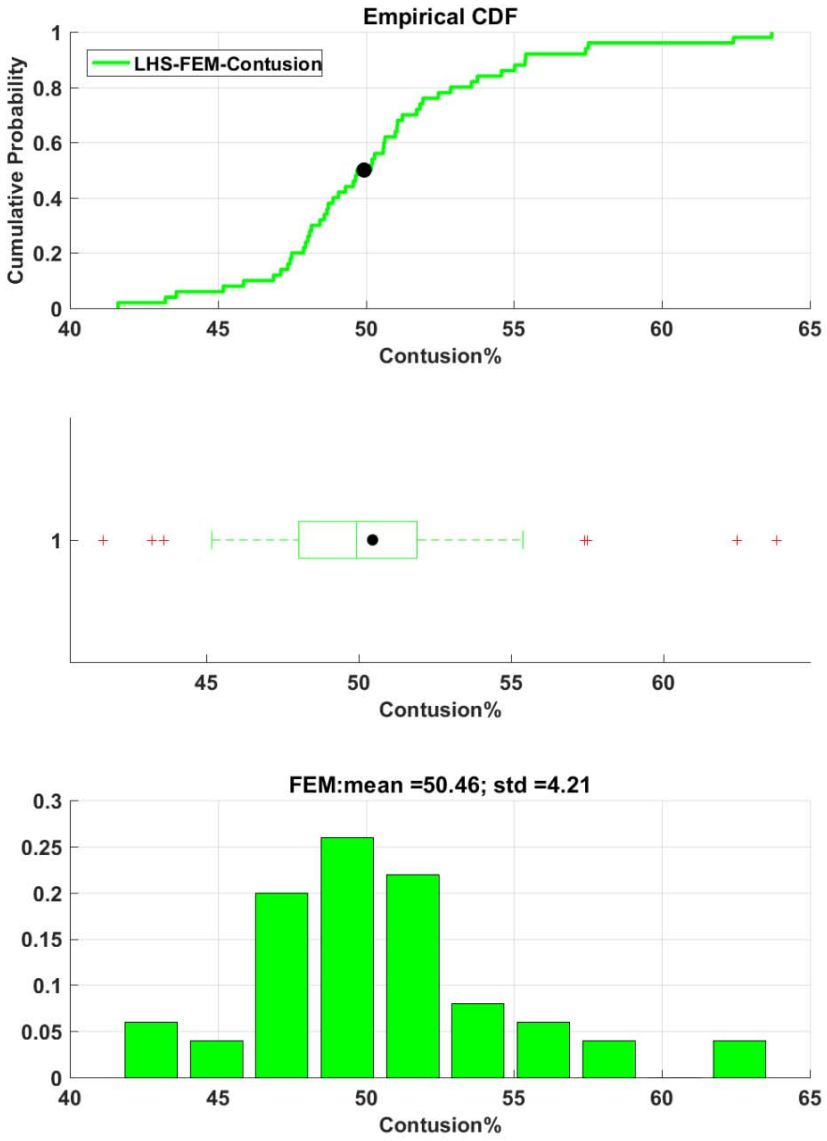

Figure 17 The uncertainty analysis with CDF, boxplot, and histogram for contusion percentage based on the 50 FEM simulations subject to LHS inputs. The values for mean and standard deviation are given in the title of the subfigure with the histogram. The mean is also indicated with the black dots in the CDFs and boxplots.

3.2.3 Sensitivity Analysis

For sensitivity analysis, scatterplots and rank correlation are used to assess the effects of individual input parameters on output responses. Scatterplots plot the paired input and output and reveal the relationships between the input parameters and output responses. The rank correlation measures the strength of the linear relationship between the input parameters and the output responses; it is calculated with a function in MATLAB. The sign of the rank correlation indicate the positive (with a "+" sign) or the negative (with a "–" sign) relationship between the input and output, and the absolute value of the rank correlation indicates how strong the linear relationships are. For example, 1 would indicate a perfect linear relationship, 0 would indicate no linear relationship.

Scatterplots for peak energy density, contact force, rib stress, and contusion paired with the properties of muscle and skin, rib, and lung are given in Figure 18, Figure 19, Figure 20, and Figure 21 respectively. In order to compare the scatterplots with the line plots got from RSM, the scatterplots carry the same color code for muscle and skin, rib, and lung. The rank correlations among these input parameters and output responses are given in Table 7 and the highest absolute value for each of the output responses in bold.

For peak energy density, the most sensitive input parameter is the properties of muscle-skin as it carries the most highest absolute value of rank correlation. This aligns with the sensitivity analysis in RSM (Table 6). All three of the input parameters (properties of muscle-skin, rib, and lung) carry negatively correlated relationships to the PED as indicated with the negative signs in the first column of Table 7, which is consistent with the negative slopes of the lines in Figure 9.

The properties of rib is the most (linear) sensitive input parameter to the contact force based on the rank correlation. However, the rank correlation does not reveal the nonlinear relationship between the input parameters and output responses, as shown in the top panel of Figure 19, the properties of muscle-skin exhibits a parabolic relationship to the contact force, and matches with the plots of Figure 10. The input parameters of rib and lung carry positive relationships to the contact force as indicated with the positive values in the second column of Table 7, which is consistent with the positive slopes of the lines for rib and lung in Figure 10.

The most (linear) sensitive input parameter to the rib stress is the property of rib as indicated with a value of 0.85 in the third column of Table 7. Indeed, a clear positive linear trend is shown in the second subplot of Figure 20, matching with the blue line in Figure 11. The sensitivity analysis that rib property is the most sensitive parameter to the rib stress is given by both RSM analysis and LHS FEM simulations.

The most (linear) sensitive parameter to the contusion is the properties of muscle-skin, whereas the property of rib (linear) is the next most sensitive. Both have a negative relationship with the contusion, which matches with the trend of the scatterplots (the top two panels of Figure 21) and the lines with the negative slopes in Figure 12. As the rank correlation only reveal linear relationships, it could not provide the interaction and higher order effects. Further assessment is needed to reveal these effects.

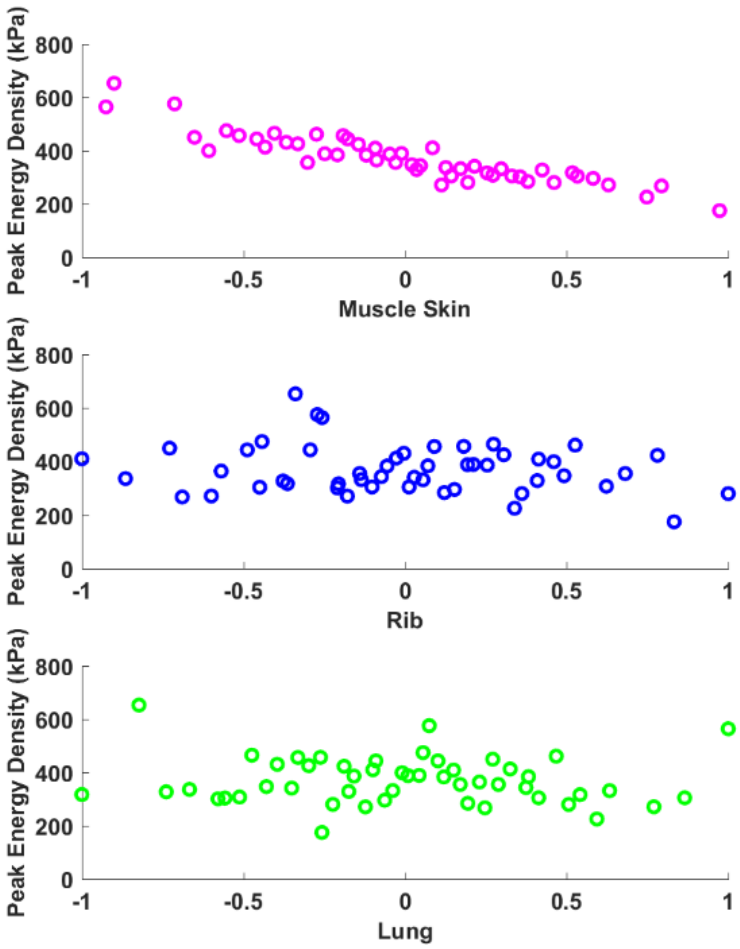

Figure 18 Scatterplot of peak energy density vs. material properties of muscle-skin, rib, and lung.

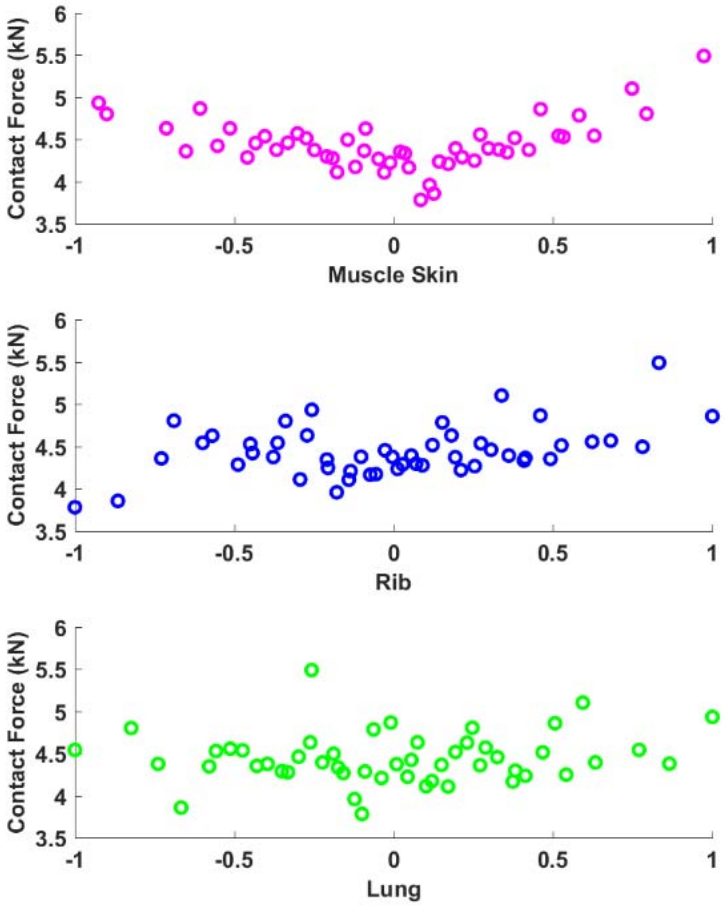

Figure 19 Scatter plot of peak contact force vs. material properties of muscle-skin, rib, and lung

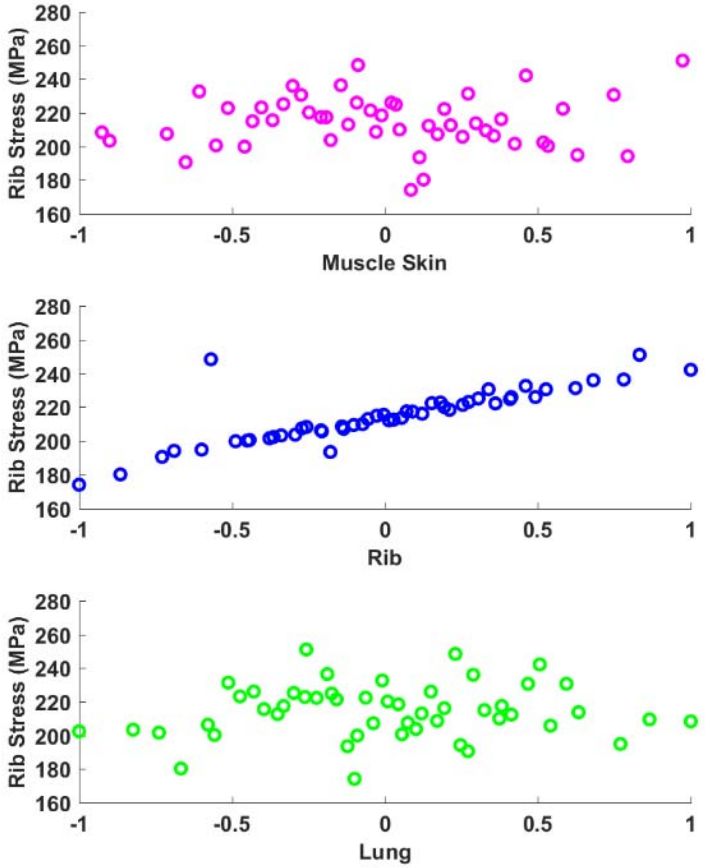

Figure 20 Scatter plot of peak rib stress vs. material properties of muscle-skin, rib, and lung

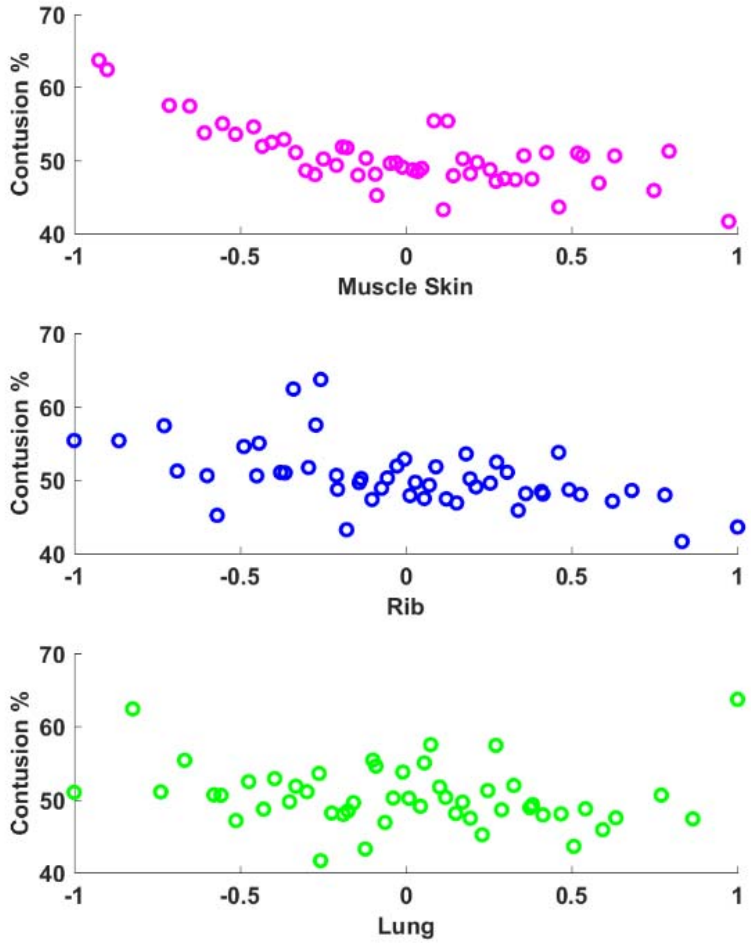

Figure 21 Scatter plot of contusion percentage vs. material properties of muscle-skin, rib, and lung

Table 7 Rank Correlation

	PED	Contact Force	Rib Stress	Contusion
Muscle-skin	**-0.91**	0.14	0.04	**-0.69**
Rib	-0.18	**0.41**	**0.85**	-0.53
Lung	-0.08	0.12	0.09	-0.13

3.3 Effect of Projectile Speed on the Uncertainty Analysis

In above analysis reported in Section 3.1 (RSM analysis) and Section 3.2 (LHS analysis), the projectile speed for lung impact was set to 40 m/s in all FEM simulations. In this section, we explore the effect of projectile speed on the uncertainty analysis for lung impact and liver impact. The values of the mean, the standard deviation, and the coefficient of variation (i.e., the ratio of

the standard deviation over the mean) are used to quantify the uncertainty under different projectile speeds.

3.3.1 Effect of Projectile Speed on Uncertainty Analysis for Lung Impact

To explore the effect of speed on the uncertainty of the output responses for lung impact, projectile speeds of 20 m/s and 30 m/s were simulated using the same LHS inputs as described in Section 3.2.1 (speed of 40 m/s). The values of the mean, the standard deviation, and the coefficient of variation are used to quantify the uncertainty for the output response under different projectile speeds. See Figure 22. The value of the mean is represented by the black dots and the error bars represent the standard deviation; the numbers next to the error bars are the coefficient of variation. For projectile speeds of 20 and 30 m/s, the sampling step for the contact force was set to 1e-5 s instead of 5e-5 s (i.e., the sample rate was set to 100 kHz instead of 20 kHz), and five points average filtering was used to get an averaged peak contact force for the FEM simulations.

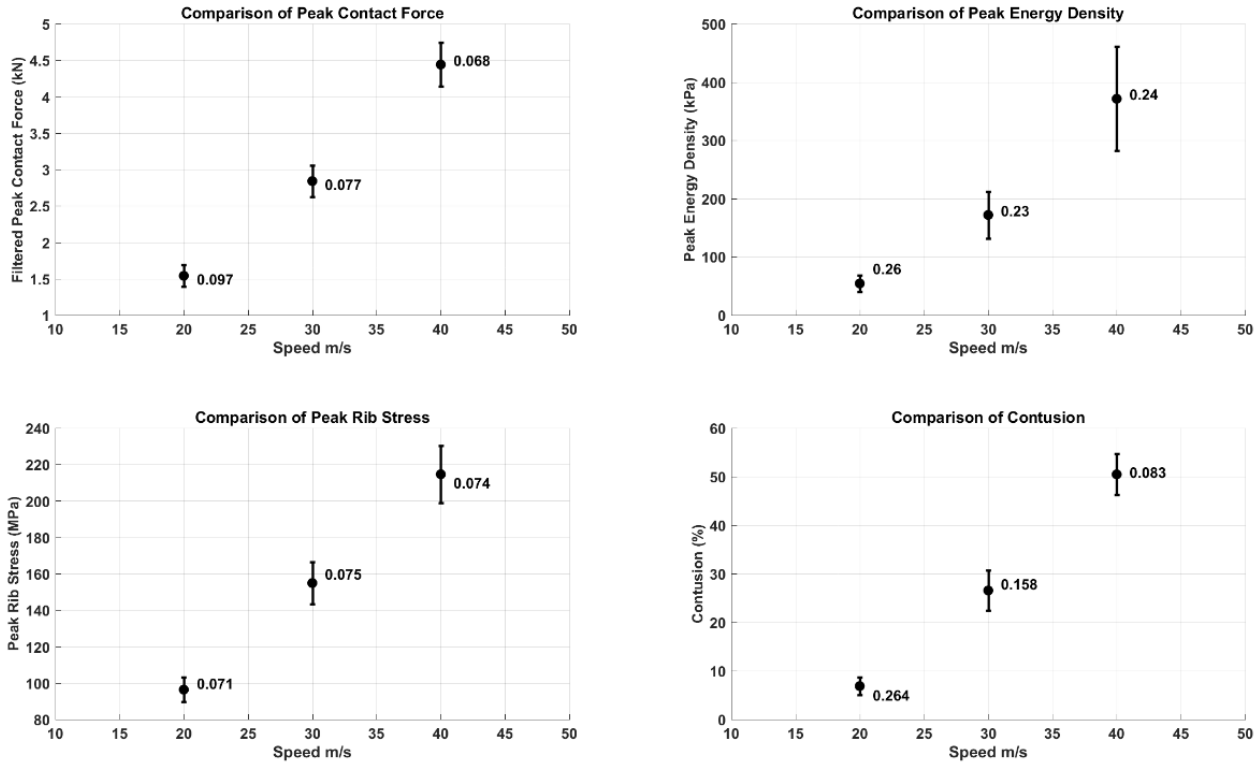

Figure 22 Projectile speed effect on the uncertainty analysis in lung impact. The values next to the error bar are the coefficient of variation (i.e., the ratio of the standard deviation to the mean) of the responses specified on the labels of y-axes.

The coefficient of variation for the peak of contact force (the panel on the top left) decreases as the projectile speed increases. The coefficient of variation for the peak energy density (the panel on the top right) does not vary with speed despite increases in the error with speed. The coefficient of variation for the peak rib stress (the panel on the bottom left) does not vary significantly with projectile speed despite slight increases in the error with speed. The coefficient of variation for

the contusion percentage (the panel on the bottom right) decreases when the projectile speeds increases, and the error bar increases slightly for speeds of 30 m/s and 40 m/s compared to that of the speed of 20 m/s.

3.3.2 Projectile Speed Effect on Uncertainty Analysis for Liver Impact

To explore the effect of speed on the uncertainty of the output responses for impact over the liver, projectile speeds of 30 m/s, 40 m/s, and 50 m/s were simulated using the same LHS inputs as described in Section 3.2.1. The liver is modeled as Ogden Rubber with the keyword of "*MAT_OGDEN_RUBBER" in LS-DYNA. The equations for calculating the liver properties are given as follows: Mu1=G1=a*exp(b*x), G2=p2*x^2+p1*x+p0, a=24.74; b=2.09, p2=0.5, p1=2.5, p0=3.

The effect of projectile speed on uncertainty analysis for liver impact is shown in Figure 23. Ten output responses are analyzed: energy density (kPa), VM-stress (kPa), effective strain, pressure (kPa), principal stress (kPa), principal strain, laceration percentage, peak contact force (kN), time of peak contact force, and rib stress (MPa). The values of the mean, the standard deviation, and the coefficient of variation are used to quantify the uncertainty for the output response under different projectile speeds. In Figure 23, the value of the mean is represented by the black dots and the error bars represent the standard deviations, the numbers next to the error bars are the coefficient of variation.

The coefficient of variation of PED (the top left panel of Figure 23) varies as the projectile speed increases; the standard deviation increases slightly with increase in speed. The mean values of PED increase with speed. The coefficient of variation of VM-stress (the top right panel of Figure 23) decreases slightly with increasing projectile speed, while the standard deviation increases slightly with speed. The mean values of the VM-stress increase with speed.

The coefficient of variation of effective strain (EStrain) (the second panel on the left in Figure 23) remains constant as the projectile speed increases, while the standard deviation increases slightly with speed. The mean values of the effective strain increase with speed.

The coefficient of variation for pressure (the second panel on the right in Figure 23) remains constant as the projectile speed increases, while the standard deviation increases slightly with speed. The mean values of the pressure increase with speed.

The coefficient of variation of principal stress (PStress) (the third panel on the left in Figure 23) decreases slightly with increasing projectile speed, while the standard deviation increases slightly with speed. The mean values of the principal stress increase with speed.

The coefficient of variation and the standard deviation of principal strain (PStrain) (the third panel on the right in Figure 23) remain constant as the projectile speed increases. The mean values of the principal strain increase with speed.

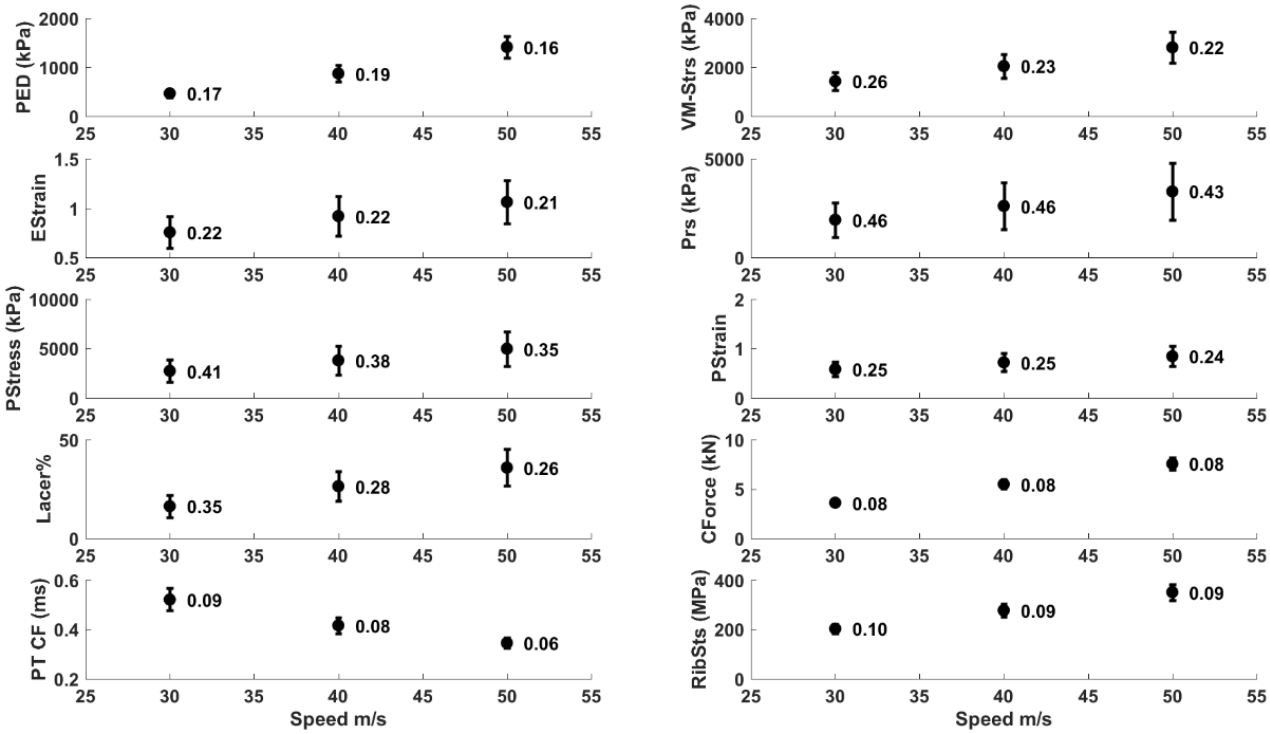

Figure 23. The effect of projectile speed on uncertainty analysis for liver impact. The values next to the error bar are the coefficient of variation of the responses (y-axis). The panels from top left to top right to bottom left and bottom right show the peak responses of energy density (kPa), von Mises stress (kPa), effective strain, pressure (kPa), principal stress (kPa), principal strain, laceration%, contact force (kN) , time of peak contact force (ms), and rib stress (MPa).

Principal stress of 189 kPa is used as the liver laceration threshold. The injured volume is obtained by adding up the volume of all elements whose principal stress are above the threshold. The injured volume over the whole volume of the liver is defined as the laceration percentage. The coefficient of variation for laceration percentage (the 4th panel on the left in Figure 23) decreases with increasing projectile speed; and the standard deviation increases slightly with speed. The mean values of the laceration percentage increase with speed. For liver impact simulations, the sampling step for the contact force was set to 1e-5 s (i.e., the sample rate was set to 100 kHz). The contact force time history was filtered using a five point average. The peak from filtered time history compared very closely to the peak form unfiltered time history, as reflected in similar coefficient of variations. The subplot of contact force here is based on the original peak value of contact force. The mean, the standard deviation, and the coefficient variation are the same cross the different speeds.

For the peak time of contact force (PT CF), the standard deviation of the peak time (the bottom left panel in Figure 23) decreases when the speed increases as does the coefficient variation and the mean.

The coefficient variation of rib stress (the bottom right panel in Figure 23) remains fairly constant with speed, while the standard deviation increases slightly with speed. The mean rib stress increases with speed.

4 Discussion

In this uncertainty and sensitivity study, we explored how the uncertainty in the input (biomechanical properties) propagated to the FE output responses, and how much the responses were affected as the input parameters were varied within realistic ranges. As shown in Figure 4, there is a large variability in stress-strain response obtained from literature [7], thus the uncertainty and sensitivity of output due to these variations were explored. The RSM and LHS approaches were taken. The input parameters were the mechanical properties of muscle and skin, rib, and lung. The output responses were the peak energy density, contact force, rib stress, and the lung contusion percentage.

In RSM, we used a face-centered CCD to select the combinations of the boundary (extreme or edge) material properties for the FEM simulations. A quadratic regression fitting function in MATLAB was used to fit the response surface models to the output of FEM. We statistically analyzed the goodness of fit and the significance of the fitted coefficients with their p-values. We quantified the uncertainty with the CDF, boxplot, histogram, the mean, and the standard deviation for both methods. For the sensitivity analysis, we used p-values and fitted line plots drawn with the response surface models to identify which parameters were most sensitive to the output response. We explored the first order and second order of single parameters, and interactions between parameters.

In LHS, 50 samples of input parameters were selected based on a truncated Gaussian distribution. We quantified the uncertainty with the CDF, boxplot, histogram, the mean and the standard deviation. We used scatter plots and rank correlation to analyze the sensitivity.

Due to the fact that CCD used only 19 combined boundary (extreme or edge) cases, it is difficult to reach a statistically meaningful uncertainty quantification. However, the results of uncertainty (especially the mean values and the trend of CDFs) were comparable to those from the 50 simulations with LHS inputs. Additionally, the upper bounds and lower bounds of the responses obtained with the two methods were very close (see Table 8 and Table 9), although some difference was seen in the contact force response. This is a good indicator that these two methods are comparable. A primary reason for this similarity is that the boundaries of the inputs for these two methods are the same, although the specific combinations are not.

Table 8 Bounds from RSM Analysis

	Energy Density (kPa)	Contact Force (kN)	Rib Stress (MPa)	Contuse Percentage
mean	407.44	4.78	211.34	54.09
max	710.60	5.66	262.87	66.40
min	177.74	3.74	174.92	41.15
(max-mean)/mean*100	74.41	18.36	24.38	22.75
(min-mean)/mean*100	-48.88	-10.08	-17.45	-17.30

Table 9 Bounds from LHS Analysis

	Energy Density (kPa)	Contact Force (kN)	Rib Stress (MPa)	Contuse Percentage
mean	371.26	4.44	214.61	50.46
max	653.15	5.49	251.10	63.71
min	174.95	3.78	174.17	41.63
(max-mean)/mean*100	75.93	23.55	17.00	26.26
(min-mean)/mean*100	-52.88	-14.92	-18.84	-17.50

Sensitivity analysis using RSM was able to provide an assessment of first order and higher order terms as well as interaction between terms. A similar analysis could have been performed using the LHS method if one treated the output arrays accordingly to find the second order and interaction effect. In this study, scatterplots from LHS helped to visualize the relationship between input and output. They were comparable with the fitted lines obtained in the RSM analysis.

The value of the mean response and the base response in the 19 combined boundary (extreme) cases in the RSM analysis are equivalent (see the boxplots of Figure 5, Figure 6, Figure 7, and Figure 8). It was not expected that these values be equivalent due to the non-linear nature of the stress-strain curves as a function of strain-rate (see Figure 4). Additionally, the FEM simulation utilizes nonlinear equations to calculate the variation of material properties from the softest to stiffest curves (see Table 3). The variation of material properties are propagated from the initial input parameters to the responses. In fact, this is a large reason for studying how uncertainty in input parameters translates to the final output responses.

In general, the uncertainty study showed that for lung impacts from a projectile speed of 40 m/s, the coefficient of variation was relatively small (~0.08) for the contact force, rib stress, and contusion. The PED had a higher coefficient of variation of 0.24. As the speed was varied, the coefficients did not change with the exception of the contusion, in which the coefficients of variation increased to 0.26 at 20 m/s. See Figure 22. The uncertainty analysis of the liver showed similar results (Figure 23). To quantify the uncertainty further, the CDF distributions can be fit.

One of the next steps to this study is to perform a sensitivity analysis for liver impacts in a similar fashion as that for the lung impact. We will explore the effect of speed on sensitivity by drawing the scatterplots and calculating the rank correlations as we did for impact speed of 40 m/s for cases of lung impact. For liver impact, we will also plot the scatter plots and calculate the rank analysis for different speed conditions. Surface response analysis on 19 extreme cases will also be performed.

To further analyze the sensitivity for lung impact and liver impact, we can use other mathematical and statistical methods as suggested in [13] (e.g., Sobol indices). As discussed above, rank correlation could be calculated with quadratic terms or interaction terms; it is likely that they provide the similar information as in RSM analysis.

Lastly, in future analysis, LHS of inputs can be based on a uniform distribution or other distribution types rather than a truncated Gaussian to explore how much responses vary with the distribution type. However, it is not expected that there will be a large difference in the responses, given the current results do not show significant differences between the inputs chosen using a truncated Gaussian distribution and inputs based upon face-centered CCD with

the RSM approach (i.e., only boundary conditions are considered, no distribution needs to be assumed).

5 Conclusions

The following conclusions can be drawn based on the results presented in this study:

(1) RSM can be used as a tool for uncertainty and sensitivity analysis for 3-factor cases. The advantage of RSM is that it needs fewer simulations and provides not only the sensitivity of the input parameters but also the sensitivity of higher order variables and of interactions between input parameters.

(2) LHS method is a more rigorous approach, and is especially applicable for complex models with more than 3 factors. LHS can be used to explore uncertainty quantification and sensitivity analysis.

(3) The sensitivity analysis based on RSM and LHS produced the same conclusion for the case of lung impact under the projectile speed of 40 m/s. Specifically, the most sensitive first order parameters for PED, contact force, rib stress, and contusions were the muscle-skin, rib, rib, and muscle-skin, respectively.

(4) RSM analysis provided additional sensitivity information for higher order parameters and interaction of input parameters. For second order input properties, the contact force and contusion were most sensitive to the second order of the properties of muscle-skin. For interaction between parameters, the PED, the contact force, and the contusion percentage, showed greatest sensitivity to the interaction of muscle-skin and rib.

(5) Both lung impact and liver impact simulations with different projectile speeds show that there is a consistency in uncertainty analysis. For both lung impact and liver impact, the standard deviations of the responses increase with speed, but the coefficient variations do not change too much with the speed. In other words, the projectile speed does not appear to be a significant factor for uncertainty analysis, as reflected in the coefficients of variation. However, this should be confirmed with other organ impact simulations.

(6) The effect of projectile speed on sensitivity analysis requires further analysis and simulations before a conclusion can be reached.

(7) The two methods of RSM and LHS provide comparable sensitivity analysis results for the case of impact over the lung region. They support and complement each other.

6 References

1. Helton, J.C. and F.J. Davis, *Latin Hypercube Sampling and the Propagation of Uncertainty in Analyses of Complex Systems.* Reliability Engineering and System Safety, 2003. **81**: p. 23-69.

2. Saltelli, A., *Sensitivity analysis for importance assessment.* Risk Anal, 2002. **22**(3): p. 579-90.

3. Box, G.E.P. and K.B. Wilson, *On the Experimental Attainment of Optimum Conditions.* Journal of the Royal Statistical Society. Series B (Methodological), 1951. **13**(1): p. 1-45.

4. McKay, M.D., R.J. Beckman, and W.J. Conover, *A Comparison of Three Methods for Selecting Values of Input Variables in the Analysis of Output from a Computer Code.* Technometrics, 1979. **21**(2): p. 239-245.

5. USEPA, *Guiding Principles for Monte Carlo Analysis*, 1997, Risk Assessment Forum; U.S. Environmental Protection Agency: Washington, DC.

6. Khan, A.A., L. Lye, and T. Husain, *Latin Hypercube Sampling for Uncertainty Analysis in Multiphase Modeling.* J. Environ. Eng. Sci., 2008. **7**: p. 617-626.

7. Niu, E., K. Mathews, and C. Webber, *Literature Review of Human Torso Properties, Finite Element Model Development and Validation*, 2018. Report J0511-18-721 (Contract N00174-17-C-0003).

8. Shen, W., et al., *Development and validation of subject-specific finite element models for blunt trauma study.* J Biomech Eng, 2008. **130**(2): p. 021022.

9. Myers, R.H., et al., *Response Surface Methodology: A Retrospective and Literature Survey.* Journal of Quality Technology, 2004. **36**(1): p. 53-77.

10. Box, G.E.P., J.S. Hunter, and W.G. Hunter, *Statistics for experimenters : design, innovation, and discovery*. 2nd edition ed. 2005, Hoboken, N.J.: Wiley-Interscience.

11. Baggs , G. *Process Development and Control in Metal Additive Manufacturing*. 2018 [cited 2018 Oct. 22]; Available from: http://www.moog.com/news/blog-new/GeorgeBaggsonAdditiveManufacturing.html

12. Ye, K.Q., W. Li, and A. Sudjianto, *Algorithmic Construction of Optimal Symmetric Latin Hypercube Designs.* Journal of Statistical Planning and Inferences, 2000. **90**(1): p. 145-159.

13. Helton, J.C., *Sampling-Based Methods for Uncertainty and Sensitivity Analysis*. Sensitivity Analysis of Model Output, ed. K.M. Hanson and F.M. Hemez. 2005: Los Alamos National Laboratory.